CHAPTER 10

RADIATION SPECTROSCOPY WITH SCINTILLATORS

In the early 1950s, the development of thallium-activated sodium iodide as a scintillation material ushered in the modern era of gamma ray spectroscopy. With its introduction, a practical detector was available which could provide a high efficiency for the detection of gamma rays, and at the same time, was capable of sufficiently good energy resolution to be useful in separating the contribution of polyenergetic gamma ray sources. Gamma ray spectroscopy using scintillators has since developed into a mature science with applications in an impressive array of scientific fields.

Despite the fact that it was virtually the first practical solid detection medium used for gamma ray spectroscopy, NaI(Tl) remains the most popular scintillation material for this application. This extraordinary success stems from its extremely good light yield, excellent linearity, and the high atomic number of its iodine constituent. Other scintillators mentioned in Chapter 8, notably cesium iodide, have also achieved some success in gamma ray spectroscopy, but the combined use of all other materials extends to only a small fraction of the cases in which sodium iodide is found. In the sections that follow, we will therefore concentrate on NaI(Tl), with the understanding that most of the discussion and general conclusions can be extended to other scintillation materials by taking into account the differences in their gamma ray interaction probabilities and scintillation properties.

Useful textbook reviews of scintillation spectroscopy of gamma radiation have been published by Birks[1], Shafroth[2], and Siegbahn[3].

I. GENERAL CONSIDERATIONS IN GAMMA RAY SPECTROSCOPY

An X- or gamma ray photon is uncharged and creates no direct ionization or excitation of the material through which it passes. The detection of gamma rays is therefore critically dependent on causing the gamma ray photon to undergo

an interaction that transfers all or part of the photon energy to an electron in the absorbing material. These interaction processes are detailed in Chapter 2, and represent sudden and major alterations of the photon properties, as opposed to the continuous slowing down of charged particles or electrons through many simultaneous interactions.

Because the primary gamma ray photons are "invisible" to the detector, it is only the fast electrons created in gamma ray interactions that provide any clue to the nature of the incident gamma rays. These electrons have a maximum energy equal to the energy of the incident gamma ray photon, and will slow down and lose their energy in the same manner as any other fast electron, such as a beta particle. Energy loss is therefore through ionization and excitation of atoms within the absorber material, and through bremsstrahlung emission (see Chapter 2).

In order for a detector to serve as a gamma ray spectrometer, it must carry out two distinct functions. First, it must act as a conversion medium in which incident gamma rays have a reasonable probability of interacting to yield one or more fast electrons, and second, it must function as a conventional detector for these secondary electrons. In the discussion that follows, we will first assume that the detector is sufficiently large so that the escape of secondary electrons (and any bremsstrahlung created along their track) is not significant. For incident gamma rays of a few MeV, the most penetrating secondary electrons will also be created with a few MeV kinetic energy. The corresponding range in typical solid detector media is a few millimeters (most bremsstrahlung photons generated along the electron track will be considerably less penetrating). The assumption of complete electron absorption, therefore, implies a detector whose minimum dimension is at least about a centimeter. Then only a small fraction of the secondary electrons, which are created more-or-less randomly throughout the volume of the detector, lie within one range value of the surface and could possibly escape. Later in this chapter we will discuss the complicating effects of electron and bremsstrahlung escape in small detectors as a perturbation on the simpler model that follows.

The following discussions will be kept relatively general so that they apply not only to other scintillation materials, but also to other solid or liquid detection media used in gamma ray spectroscopy. Chapters 12 and 13 discuss semiconductor detectors which have been widely applied to gamma ray spectroscopy over the past decade. The following section will also serve as a general introduction to these chapters, because the basic modes of gamma ray interactions are identical for all detector types.

The requirement of full absoroption of the secondary electron rules out gas-filled detectors for the spectroscopy of gamma rays, other than those with very low energy. The penetration distance of a 1 MeV electron in STP gases is several meters, so that detectors of any practical size can never come close to absorbing all the secondary electron energy. To further complicate the situation,

most gamma ray induced pulses from a gas-filled counter arise from gamma ray interactions taking place in the solid counter wall, following which the secondary electron finds its way to the gas before being fully stopped. Under these conditions, the electron loses a variable and an indeterminant amount of energy in the wall, which does not contribute to the detector output pulse, and therefore virtually all hope of relating the electron to incident gamma ray energy is lost.

II. GAMMA RAY INTERACTIONS

Of the various ways gamma rays can interact in matter, only three interaction mechanisms have any real significance in gamma ray spectroscopy: photoelectric absorption, Compton scattering, and pair production. As detailed in Chapter 2, photoelectric absorption predominates for low-energy gamma rays (up to several hundred keV), pair production predominates for high-energy gamma rays (above 5–10 MeV), and Compton scattering is the most probable process over the range of energies between these extremes. The atomic number of the interaction medium has a strong influence on the relative probabilities of these three interactions, as can be seen from the formulae and plots given in Chapter 2. The most striking of these variations involves the cross section for photoelectric absorotion, which varies approximately as $Z^{4.5}$. As we will see from the following discussion, because photoelectric absorption is the preferred mode of interaction, there is a premium on choosing detectors for gamma ray spectroscopy from materials that incorporate elements with high atomic number.

A. Photoelectric Absorption

Photoelectric absorption is an interaction in which the incident gamma ray photon disappears. In its place, a photoelectron is produced from one of the electron shells of the absorber atom with a kinetic energy given by the incident photon energy $h\nu$ minus the binding energy of the electron in its original shell (E_b). This process is shown in the diagram below. For typical gamma ray energies, the photoelectron is most likely to emerge from the K shell, for which typical binding energies range from a few keV for low-Z materials, to tens of keV for materials with higher atomic number.

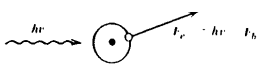

The vacancy that is created in the electron shell as a result of the photoelectron emission is quickly filled by electron rearrangement. In the process, the binding energy is liberated either in the form of a characteristic X-ray or Auger

electron. In iodine, a characteristic X-ray is emitted in about 88 percent of the cases[4]. The Auger electrons have extremely short range because of their low energy. The characteristic X-rays may travel some distance (typically a millimeter or less) before being reabsorbed through photoelectric interactions with less tightly bound electron shells of the absorber atoms. Although escape of these X-rays can at times be significant, for now we will assume that they are also fully absorbed in keeping with our simplified model.

Thus, the effect of photoelectric absorption is the liberation of a photoelectron, which carries off most of the gamma ray energy, together with one or more low-energy electrons corresponding to absorption of the original binding energy of the photoelectron. If nothing escapes from the detector, then the sum of the kinetic energies of the electrons that are created must equal the original energy of the gamma ray photon.

Photoelectric absorption is therefore an ideal process if one is interested in measuring the energy of the original gamma ray. The total electron kinetic energy equals the incident gamma ray energy, and will always be the same if monoenergetic gamma rays are involved. Under these conditions, the differential distribution of electron kinetic energy for a series of photoelectric absorption events would be a simple delta function as shown below. The single peak appears at a total electron energy corresponding to the energy of the incident gamma rays.

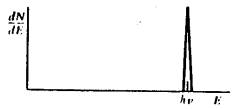

B. Compton Scattering

The result of a Compton scattering interaction is the creation of a recoil electron and scattered gamma ray photon, with the division of energy between the two dependent on the scattering angle. A sketch of the interaction is given below.

The energy of the scattered gamma ray $h\nu'$ in terms of its scattering angle θ is given by

$$h\nu' = \frac{h\nu}{1 + \frac{h\nu}{m_0c^2}(1 - \cos\theta)} \tag{10-1}$$

where m_0c^2 is the rest mass energy of the electron (0.511 MeV). The energy of the recoil electron is therefore

$$E_e = h\nu - h\nu' = h\nu \left[\frac{\frac{h\nu}{m_0c^2}(1 - \cos\theta)}{1 + \frac{h\nu}{m_0c^2}(1 - \cos\theta)} \right] \tag{10-2}$$

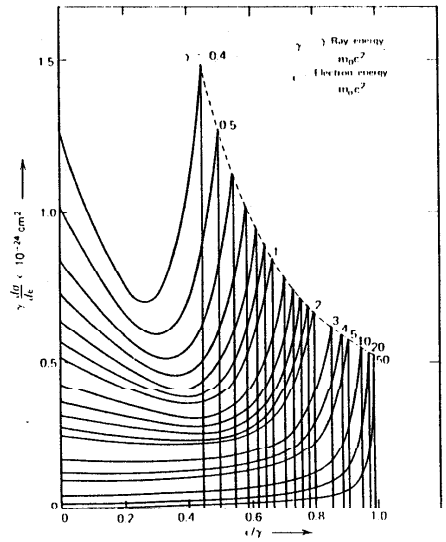

FIGURE 10-1. Shape of the Compton continuum for various gamma ray energies. (From S. M. Shafroth, ed., *Scintillation Spectroscopy of Gamma Radiation.* (Copyright 1964 by Gordon and Breach, Inc. By permission of the publisher.)

Two extreme cases can be identified:

1. A grazing angle scattering, or one in which $\theta \simeq 0$. In this case, Eqs. 10-1 and 10-2 predict that $h\nu' \simeq h\nu$ and $E_e \simeq 0$. In this extreme, the recoil Compton electron has very little energy and the scattered gamma ray has nearly the same energy as the incident gamma ray.
2. A head-on collision in which $\theta = \pi$. In this extreme, the incident gamma ray is backscattered toward its direction of origin, whereas the electron recoils along the direction of incidence. This extreme represents the maximum energy that can be transferred to an electron in a single Compton interaction. Equations 10-1 and 10-2 yield for this case

$$h\nu']_{\theta=\pi} = \frac{h\nu}{1 + 2\frac{h\nu}{m_0c^2}} \tag{10-3}$$

$$E_e]_{\theta=\pi} = h\nu \left[\frac{2h\nu/m_0c^2}{1 + 2h\nu/m_0c^2} \right] \tag{10-4}$$

In normal circumstances, all scattering angles will occur in the detector. Therefore, a continuum of energies can be transferred to the electron, ranging from zero up to the maximum predicted by Eq. 10-4. Figure 10-1 shows the shape of the distribution of Compton recoil electrons predicted by the Klein-Nishina cross section (Chapter 2) for several different values of the incident gamma ray energy. For any one specific gamma ray energy, the electron energy distribution has the general shape shown in the sketch below.

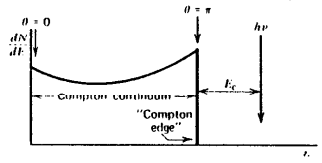

The gap between the maximum Compton recoil electron energy and the incident gamma ray energy is given by

$$E_e = h\nu - E_e]_{\theta=\pi} = \frac{h\nu}{1 + 2h\nu/m_0c^2} \tag{10-5}$$

In the limit that the incident gamma ray energy is large, or $h\nu \gg m_0c^2/2$, this energy difference tends toward a constant value given by

$$E_e \cong \frac{m_0c^2}{2} \ (=0.256 \text{ Mev}) \tag{10-6}$$

The preceding analysis is based on the assumption that Compton scattering involves electrons that are intitially free or unbound. In actual detector materials, the binding energy of the electron prior to the scattering process can have a measureable effect on the shape of the Compton continuum. These effects will be particularly noticeable for low incident gamma ray energy. They involve a rounding-off of the rise in the continuum near its upper extreme, and the introduction of a finite slope to the abrupt drop of the Compton edge. These effects are often masked by the finite energy resolution of the detector, but can be evident in the spectra from detectors with high inherent resolution (see Fig. 13-8).

C. Pair Production

The third significant gamma ray interaction is pair production. The process occurs in the field of a nucleus of the absorbing material, and corresponds to the creation of an electron-positron pair at the point of complete disappearance of the incident gamma ray photon. Because an energy of $2m_0c^2$ is required to create the electron-positron pair, a minimum gamma ray energy of 1.02 MeV is required to make the process energetically possible. If the incident gamma ray energy exceeds this value, the excess energy appears in the form of kinetic energy shared by the electron-positron pair. Therefore, the process consists of converting the incident gamma ray photon into electron and positron kinetic energies which total

$$E_e + E_{e'} = h\nu - 2m_0c^2 \tag{10-7}$$

For typical energies, both the electron and positron travel a few millimeters at most before losing all their kinetic energy to the absorbing medium. A plot of the total (electron + positron) charged particle kinetic energy created by the incident gamma ray is again a simple delta function, but it is now located $2m_0c^2$ below the incident gamma ray energy, as illustrated in the sketch below. In our

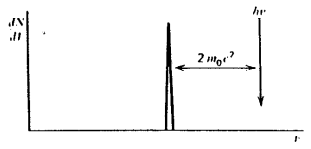

simple model, this amount of energy will be deposited each time a pair production interaction occurs within the detector.

The pair production process is complicated by the fact that the positron is not a stable particle. Once its kinetic energy becomes very low (comparable to the thermal energy of normal electrons in the absorbing material), the positron will annihilate or combine with a normal electron in the absorbing medium. At this point both disappear, and they are replaced by two annihilation gamma ray photons of energy m_0c^2 (.511 MeV) each. The time required for the positron to slow down and annihilate is small, so that the annihilation radiation appears in virtual coincidence with the original pair production interaction.

III. PREDICTED RESPONSE FUNCTIONS

A. "Small" Detectors

As an example of one extreme in gamma ray detector behavior, we first examine the expected response of detectors whose size is small compared with the mean free path of the *secondary gamma radiations* produced in interactions of the original gamma rays. These secondary radiations consist of Compton scattered gammas, together with annihilation photons formed at the end of the tracks of positrons created in pair production. Because the mean free path of the secondary gamma rays is typically of the order of several centimeters, the condition of "smallness" is met if the detector dimensions do not exceed a centimeter or two. At the same time, we will retain our original simplifying assumption that all charged particle energy (photoelectron, Compton electron, pair electron, and positron) are completely absorbed within the detector volume.

The predicted electron energy deposition spectra under these conditions are illustrated in Fig. 10-2. If the incident gamma ray energy is below the value at which pair production is significant, the spectrum results only from the combined effect of Compton scattering and photoelectric absorption. The continuum of energies corresponding to Compton scattered electrons is called the *Compton continuum*, whereas the narrow peak corresponding to photoelectrons is designated as the *photopeak*. For the "small" detector, only single interactions take place, and the ratio of the area under the photopeak to the area under the Compton continuum is the same as the ratio of the photoelectric cross section to the Compton cross section in the detector material.

If the incident gamma ray energy is sufficiently high (several M V), the results of pair production are also evident in the electron energy spectrum. For a small detector, only the electron and positron kinetic energies are deposited, and the annihilation radiation escapes. The net effect is to add a *double escape peak* to the spectrum located at an energy of $2m_0c^2$ ($\sim$1.02 MeV) below the photopeak. The term "double escape" refers to the fact that both annihilation photons escape from the detector without further interaction.

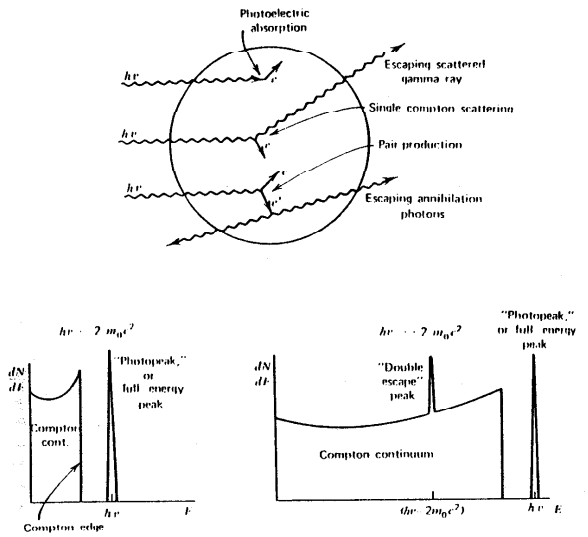

FIGURE 10-2. The "small detector" extreme in gamma ray spectroscopy. The processes of photoelectric absorption and single Compton scattering give rise to the low-energy spectrum at the left. At higher energies, the pair production process adds a "double escape" peak shown in the spectrum at the right.

B. Very Large Detectors

As an opposite extreme case, imagine that gamma rays could be introduced near the center of a very large detector, perhaps in an arrangement resembling that of Fig. 10-3. The detector dimensions are now assumed to be sufficiently large so that all secondary radiations, including Compton scattered gamma rays and annihilation photons, also interact within the detector active volume and none escape from the surface. For typical gamma ray energies, this condition would translate into requiring detector dimensions which are of the order of many tens of centimeters, unrealistically large for most practical cases.

Nonetheless, it is helpful to see how increasing the detector size greatly simplifies its response function. Some typical histories, obtained by following a

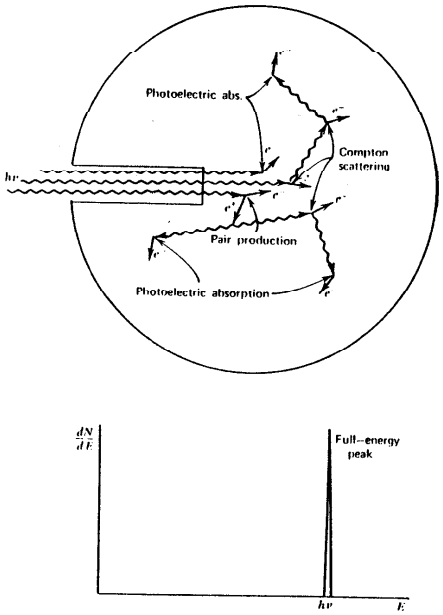

FIGURE 10-3. The "large detector" extreme in gamma ray spectroscopy. All gamma ray photons, no matter how complex their mode of interaction, ultimately deposit all their energy in the detector. Some representative histories are shown at the top.

particular source gamma ray and all subsequent secondary radiation, are sketched in Fig. 10-3. If the initial interaction is a Compton scattering event, the scattered gamma ray will subsequently interact at some other location within the detector. This second interaction may also be a Compton scattering event, in which case a scattered photon of still lower energy is produced. Eventually, a photoelectric absorption will occur and the history is terminated at that point.

It is important to appreciate the small amount of time required for the entire history to take place. The primary and secondary gamma rays travel at the speed

of light in the detector medium. If the average migration distance of the secondary gamma rays is of the order of 10 cm, the total elapsed time from start to finish of the history will be less than a nanosecond. This time is substantially less than the inherent response time of virtually all practical detectors used in gamma ray spectroscopy. Therefore, the net effect is to create the Compton electrons at each scattering point and the final photoelectron in time coincidence. The pulse produced by the detector will therefore be the sum of the responses due to each individual electron. If the detector responds linearly to electron energy, then a pulse is produced which is proportional to the *total* energy of all the electrons produced along the history. Because nothing escapes from the detector, this total electron energy must simply be the original energy of the gamma ray photon, no matter how complex any specific history may be. *The detector response is, therefore, the same as if the original gamma ray photon had undergone a simple photoelectric absorption in a single step.*

The same type of argument can be used if the history involves a pair production event. The annihilation photons formed when the positron is stopped are now assumed to interact through Compton scattering or photoelectric absorption elsewhere in the detector. Again, if the detector is large enough to prevent any secondary radiation from escaping, the sum of the kinetic energies of the electron-positron pair and subsequent Compton and photoelectrons produced by interaction of the annihilation radiation must equal the original gamma ray photon energy. Therefore, the detector response is again simply proportional to the original gamma ray energy.

The conclusion to be reached is therefore very simple: If the detector is sufficiently large and its response linearly dependent on electron kinetic energy, then the signal pulse is identical for all gamma ray photons of the same energy, regardless of the details of each individual history. This circumstance is very fortunate because the detector response function now consists of the single peak shown in Fig. 10-3 rather than the more complex function shown in Fig. 10-2. The ability to interpret complex gamma ray spectra involving many different energies is obviously enhanced when the response function consists of a single peak.

By common usage, the corresponding peak in the response function is called the "photopeak," just as in the case of the small detector. It should be realized, however, that in addition to simple photoelectric events, much more complex histories involving multiple Compton scattering or pair production also contribute pulses that fall within this peak. A better name is the *full-energy peak* because it represents all histories in which all of the original gamma ray energy is fully converted to electron kinetic energy.

C. Intermediate Size Detectors

Real detectors of the sizes in common use for gamma ray spectroscopy are neither small nor large by the standards given above. For usual geometries in which the gamma rays are incident externally on the surface of the detector,

even large-volume detectors appear finite because some interactions will take place near the entrance surface. Normal detector response functions therefore combine some of the properties discussed for the two previous cases, as well as additional features related to *partial* recovery of the secondary gamma ray energy. Some representative histories that illustrate these added possibilities are shown in Fig. 10-4, together with corresponding features in the response function.

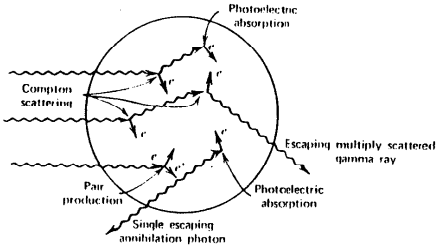

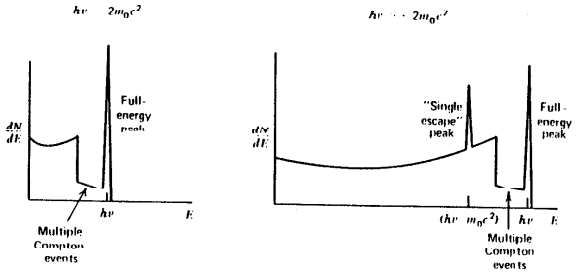

FIGURE 10-4. The case of intermediate detector size in gamma ray spectroscopy. In addition to the continuum from single Compton scattering and the full-energy peak, the spectrum at the left shows the influence of multiple Compton events followed by photon escape. The full-energy peak also contains some histories that began with Compton scattering.
At the right, the "single escape" peak corresponds to initial pair production interactions in which only one annihilation photon leaves the detector without further interaction.

The spectrum for low to medium gamma ray energies (where pair production is not significant) again consists of a Compton continuum and photopeak. Now, however, the ratio of the area under the photopeak to that under the Compton continuum is significantly enhanced over that for the very small detector due to the added contribution of multiple events to the photopeak. The lower the incident gamma ray energy, the lower will be the average energy of a Compton-scattered photon and the corresponding average distance of migration. Thus, even detectors of moderate size will appear to be large, and the relative area under the photopeak increases with decreasing incident photon energy. At very low energies (say < 100 keV) the Compton continuum may effectively disappear.

At medium energies, the possibility of multiple Compton scattering followed by escape of the final scattered photon can lead to a total energy deposition that is greater than the maximum predicted by Eq. 10-4 for single scattering. These multiple events can thus partially fill in the gap between the Compton edge and the photopeak, as well as distort the shape of the continuum predicted for single scattering.

If the gamma ray energy is high enough to make pair production significant, a more complicated situation prevails. The annihilation photons now may either escape or undergo further interaction within the detector. These additional interactions may lead to either partial or full energy absorption of either one or both of the annihilation photons.

If both annihilation photons escape without interaction, events occur that contribute to the double escape peak discussed previously. Another relatively frequent occurrence is a history in which one annihilation photon escapes but the other is totally absorbed. These events contribute to a *single escape peak* which now appears in the spectrum at an energy of m_0c^2 (0.511 MeV) below the photopeak. A continuous range of other possibilities exists in which one or both of the annihilation photons are partially converted to electron energy through Compton scattering and subsequent escape of the scattered photon. Such events accumulate in a broad continuum in the pulse height spectrum lying between the double escape peak and the photopeak.

The response function to be expected for a real gamma ray detector will depend on the size, shape, and composition of the detector, and also the geometric details of the irradiation conditions. For example, the response function will change somewhat if a point gamma ray source is moved from a position close to the detector to one which is far away. The variation is related to the differences in the spatial distribution of the primary interactions which occur within the detector as the source geometry is changed. In general, the response function is too complicated to predict in detail other than through the use of Monte Carlo calculations which simulate the histories actually taking place in a detector of the same size and composition.

Some properties of the response function are of general interest in gamma ray spectroscopy. The *photofraction* is defined as the ratio of the area under the photopeak (or full-energy peak) to that under the entire response function. It is a direct measure of the probability that a gamma ray that undergoes interaction of any kind within the detector ultimately deposits its full energy. Large values of the photofraction are obviously desirable to minimize the complicating effects of Compton continua and escape peaks in the spectrum.

At high gamma ray energies, the single and double escape peaks are quite prominent parts of the response function and can, under some circumstances, become larger than the photopeak. The ratio of the area under the single or double escape peak to the area under the photopeak is also a widely quoted property of the response function which can help in the interpretation of complex spectra.

D. Complications in the Response Function

1. SECONDARY ELECTRON ESCAPE

If the detector is not large compared with typical secondary electron ranges, a significant fraction of the electrons may leak from the detector surface and their energy will not be fully collected. This effect is enhanced for high gamma ray energies for which the average secondary electron energy is also high. Electron leakage will tend to distort the response function by moving some events to a lower amplitude from that which would be observed if the entire electron energy were collected. The shape of the Compton continuum will therefore be altered somewhat to favor lower amplitudes. Because some events will be lost from the photopeak, the photofraction will be reduced as compared with the situation in which electron leakage is not important.

2. BREMSSTRAHLUNG ESCAPE

One of the mechanisms by which secondary electrons lose energy is by the radiation of bremsstrahlung photons. The fraction lost by this process increases sharply with electron energy, and becomes the dominant process for electrons with energy over a few MeV (see Chapter 2). Even though the electron itself may be fully stopped within the detector, there is a possibility that some fraction of the bremsstrahlung photons may escape without being reabsorbed. The effects on the response function are similar to those described in the previous paragraph for electron escape, and again are most important when the incident gamma ray energy is large. For both secondary electron or bremsstrahlung escape, the effects on the response function shape are relatively subtle and broadly distributed.

3. CHARACTERISTIC X-RAY ESCAPE

In the photoelectric absorption process, a characteristic X-ray is emitted by the absorber atom. In the majority of cases this X-ray energy is reabsorbed fairly near the original interaction site. If the photoelectric absorption occurs near a surface of the detector, however, the X-ray photon may escape. In this event, the

energy deposited in the detector is decreased by an amount equal to the X-ray photon energy. Without the X-ray escape, the original gamma ray would have been fully absorbed and the resulting pulse would have contributed to the photopeak. With escape, a new category of events is created in which an amount of energy equal to the original gamma ray energy minus the characteristic X-ray energy is repeatedly deposited in the detector. Therefore, a new peak will appear in the response function, and will be located at a distance equal to the energy of the characteristic X-ray below the photopeak. These peaks are generally labeled "X-ray escape peaks" and tend to be most prominent at low incident gamma ray energies and for detectors whose surface-to-volume ratio is large. Examples are shown in the spectra of Figs. 10-10 and 13-6.

4. SECONDARY RADIATIONS CREATED NEAR THE SOURCE

Annihilation Radiation

If the gamma ray source consists of an isotope that decays by positron emission, an additional peak in the spectrum at 0.511 MeV is to be expected from the annihilation photons created when the positron is stopped. Most standard gamma ray sources are encapsulated in a covering sufficiently thick to fully stop all the positrons, and thus they undergo annihilation in the region immediately surrounding the source. This region therefore acts as a source of 0.511 MeV annihilation radiation which is superimposed on the gamma ray spectrum expected from decay of the source itself.

Bremsstrahlung

Most common gamma ray sources decay by beta-minus emission, and the source encapsulation is usually also thick enough to stop these beta particles. In other cases, an external absorber may be used to prevent the betas from reaching the detector where their energy deposition would needlessly complicate the gamma ray spectrum. In the absorption process, however, some secondary radiation in the form of bremsstrahlung will be generated and may reach the detector and contribute to the measured spectrum. In principle, the bremsstrahlung spectrum may extend to an energy equal to the maximum beta particle energy, but significant yields are confined to energies that are much lower than this value. Some examples of bremsstrahlung energy spectra are given in Fig. 10-5, which illustrates the shape of the spectrum favoring low-energy bremsstrahlung photon emission. Because these spectra are continua, they do not lead to peaks in the recorded spectra but rather can add a significant continuum upon which all other features of the gamma ray spectra are superimposed. Because the bremsstrahlung contribution cannot be simply subtracted as a background, its inclusion can lead to errors in quantitative measurements of areas under peaks in the gamma ray spectrum. In order to minimize the generation of bremsstrahlung, the use of beta absorbers made from low atomic number materials, such as beryllium, is often preferred.

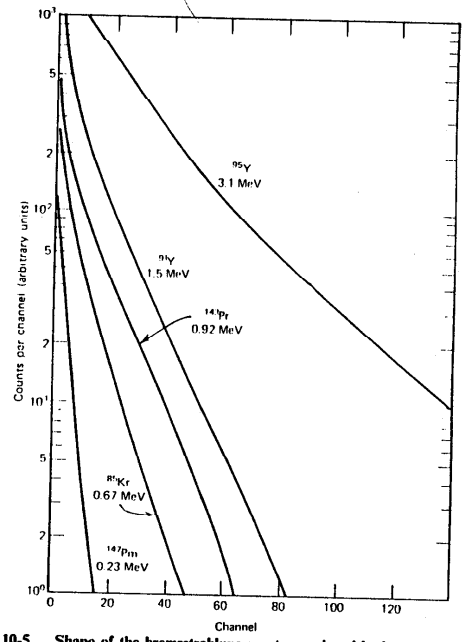

FIGURE 10-5. Shape of the bremsstrahlung spectra produced by beta particles with the indicated endpoint energies. (From Heath[5].)

5. EFFECTS OF SURROUNDING MATERIALS

In any practical application, a detector used for gamma ray spectroscopy is surrounded by other materials which can have a measurable influence on its response. At a very minimum, the detector is encapsulated to provide a barrier against moisture and light, or is mounted within a vacuum enclosure. In order to reduce natural background, most gamma ray detectors will also be operated within a shielded enclosure. The gamma ray source itself is often part of a larger sample of the material or is contained within some type of encapsulation. All of

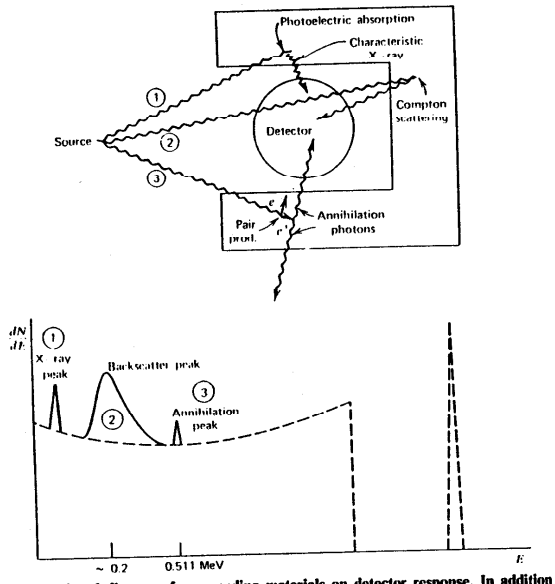

FIGURE 10-6. Influence of surrounding materials on detector response. In addition to the expected spectrum (shown as a dashed line), the representative histories shown at the top lead to the indicated corresponding features in the response function.

these materials are potential sources of secondary radiations which can be produced by interactions of the primary gamma rays emitted by the source. If the secondary radiations reach the detector, they can influence the shape of the recorded spectrum to a noticeable extent. Some possibilities are illustrated in Fig. 10-6.

Backscattered Gamma Rays

Pulse height spectra from gamma ray detectors often show a peak in the vicinity of 0.2–0.25 MeV, called the "backscatter peak." The peak is caused by gamma rays from the source which have first interacted by Compton scattering in one of the materials surrounding the detector. Figure 10-7 shows the energy depen-

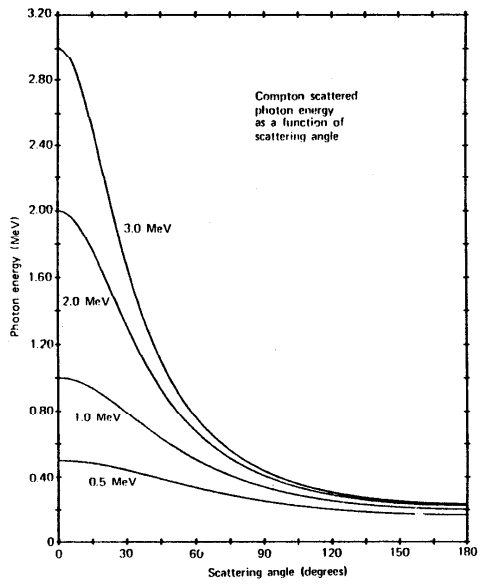

FIGURE 10-7. Variation of scattered gamma ray energy with scattering angle.

dence of these scattered gamma rays as a function of the scattering angle. From the shape of these curves, it can be seen that any scattering angle greater than about 110–120° results in scattered photons of nearly identical energy. Therefore, a monoenergetic source will give rise to many scattered gamma rays whose energy is near this minimum value, and a peak will appear in the recorded spectrum. The energy of the backscatter peak will correspond to Eq. 10-3

$$h\nu']_{\theta=\pi} = \frac{h\nu}{1 + 2h\nu/m_0c^2}$$

In the limit that the primary gamma ray energy is large ($h\nu \gg m_0c^2/2$) this

expression reduces to

$$h\nu'\big]_{\theta=\pi} \cong \frac{m_0c^2}{2} \tag{10-8}$$

Thus, the backscatter peak always occurs at an energy of 0.25 MeV or less.

Other Secondary Radiations

In addition to Compton scattering, other interactions of the primary gamma rays in the surrounding materials can give noticeable peaks in the recorded spectrum. For example, photoelectric absorption in the materials immediately surrounding the detector can lead to generation of a characteristic X-ray which may reach the detector. If the atomic number of the material is high, the X-ray photon will be relatively energetic and can penetrate significant thicknesses of intervening material. Therefore, high-Z materials should be avoided in the immediate vicinity of the detector. On the other hand, the most effective shielding materials are those with high atomic numbers such as lead. A "graded shield" is one in which the bulk of the shield is made from high-Z materials, but the inner surface is lined with a material with lower atomic number. This inner lining serves to absorb the characteristic X-ray emitted by the bulk of the shield, at the same time emitting only low energy or weakly penetrating X-rays of its own.

If the energy of the primary gamma rays is high, pair production within surrounding materials can give a significant yield of annihilation radiation. A peak can therefore appear at 0.511 MeV in the spectrum from the detection of these secondary photons. There is a danger of confusing this peak with that expected from annihilation radiation produced by radioactive sources which are positron emitters, and care must therefore be exercised in identifying the source of these annihilation photons.

E. Summation Effects

Additional peaks caused by the coincident detection of two (or more) gamma ray photons may also appear in the recorded pulse height spectrum. The most common situation occurs in applications involving an isotope which emits multiple cascade gamma rays in its decay, as illustrated in Fig. 10-8. Assuming that no isomeric states are involved, the lifetime of the intermediate state is generally so short that the two gamma rays are, in effect, emitted in coincidence. It is then quite possible for both gamma ray photons from a single decay to interact and deposit all of their energy within a time that is short compared with the response time of the detector or the resolving time of the following electronics. If enough of these events occur, a "sum peak" will be observable in the spectrum which occurs at a pulse height that corresponds to the sum of the two individual gamma ray energies. A continuum of sum events will also occur at lower amplitudes due to the summation of partial energy loss interactions.

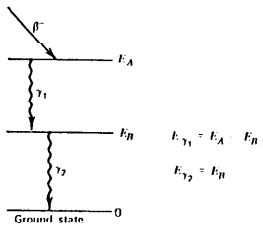

FIGURE 10-8. Simplified nuclear decay scheme which can lead to summation effects in gamma spectra. Provided the intermediate state (at E_B) is short-lived, γ_1 and γ_2 are emitted in virtual coincidence.

The relative number of events expected in the sum peak depends on the branching ratio of the two gamma rays, the angular correlation that may exist between them, and the solid angle subtended by the detector. A complete analysis is often quite complex, but the following simplified derivation illustrates the general approach that can be applied.

Let ϵ_1 be the intrinsic peak efficiency of the detector for gamma ray ①, and Ω be the fractional solid angle (steradians/4π) subtended by the detector. Then the full-energy peak area for gamma ray ① in the absence of summing effects will be

$$N_1 = \epsilon_1 \Omega S y_1 \tag{10-9}$$

where S is the number of source decays over the observation period and y_1 is the yield of gamma ray ① per disintegration. Applying the same definitions to gamma ray ②

$$N_2 = \epsilon_2 \Omega S y_2 \tag{10-10}$$

The probability of simultaneous detection of both gamma rays is the product of both individual detection probabilities, multiplied by a factor $W(0°)$ to account for any angular correlation between the gamma ray photons. $W(0°)$ is defined as the relative yield of γ_2 per unit solid angle about the 0° direction defined by the detector position, given that γ_1 is emitted in the same direction. Then the sum peak area should be

$$N_{12} = S(\epsilon_1 \Omega y_1)\cdot(\epsilon_2 \Omega y_2) W(0°)$$

$$N_{12} = S\epsilon_1\epsilon_2 y_1 y_2 \Omega^2 W(0°) \tag{10-11}$$

The summation process not only creates the sum peak, but also removes events which would otherwise fall within individual gamma ray full-energy

peaks. The remaining number of full-energy events for γ_1 is (from Eqs. 10-9 and 10-11)

$$N_1]^{\text{with}}_{\text{summation}} - N_1 \quad N_{12}$$
$$= \epsilon_1 \Omega S y_1 [1 - \epsilon_2 \Omega y_2 W(0°)] \tag{10-12}$$

Because coincident events of any kind from γ_2 (not just photopeak events) will remove a count from N_1, the detection efficiency ϵ_2 should now be interpreted as the intrinsic *total* efficiency. In order to keep these losses small, the fractional solid angle Ω is often restricted to small values to keep the second term in the above equation much smaller than the first. If the solid angle is too large, quantitative measurements based on determination of the area under full-energy peaks can be in error unless the second term is accounted for[6].

The summation process described above involves multiple radiations from the same nuclear decay event, and therefore is classified as a "true coincidence" by the definitions given in Chapter 17. Another process can also lead to summed pulses due to the accidental combination of two separate events from independent decays which occur closely spaced in time. Because the time intervals separating adjacent events are randomly distributed, some will be less than the inherent resolving time of the detector or pulse processing system. These "chance coincidences" increase rapidly with increasing counting rate, and will occur even in the absence of true coincidences. A corresponding sum peak can therefore appear in spectra from isotopes which emit only a single radiation per decay.

Chance coincidences will occur if a second pulse arrives within the resolving time t_r following a typical signal pulse. For a random pulse rate of r_s and $r_s t_r \ll 1$, the rate at which coincidences occur should be the fraction of all time which lies within t_r of a preceding pulse (given by $r_s t_r$) multiplied by the rate of pulse arrival (r_s), or

$$r_{ch} = r_s^2 t_r \tag{10-13}$$

Therefore, the accidental sum peak will have an intensity that is proportional to the square of the counting rate, whereas both the true sum peak or normal photopeaks will be linearly related to the counting rate. When multiple radiations are involved, accidental sum peaks may potentially occur at all possible combinations of any two single energies. At normal rates and typical detector solid angles, however, sum peaks are usually lost in fluctuations in the continua and background present from other energies, except at the upper energy extremes of the spectrum where such backgrounds are low.

As a practical matter, the resolving time t_r is normally set by the shaping time constants of the linear amplifier used in the pulse processing chain from the detector. The chance coincidences therefore take the form of *pulse pileup* in the amplifier, which is further detailed in the discussions of Chapter 17.

F. Coincidence Methods in Gamma Ray Spectrometers

1. CONTINUUM REDUCTION

For an ideal gamma ray detector, the response function would be simply a single well-resolved peak with no associated continuum. Weak radiations could then be most easily detected in the presence of strong interfering gamma rays of high energy, and the overall detector response to a complex gamma ray spectrum could be easily unfolded.

At the price of added complexity, some steps can be taken to more closely approach this ideal, even for gamma ray detectors with response functions that are inherently more complicated. These methods involve placing other detectors around the primary detector, and employ coincidence techniques to preferentially select those events that are most likely to correspond to full-energy absorption. For the case of sodium iodide spectrometers, the most common methods involve the use of an annular detector surrounding the primary crystal for Compton suppression by anticoincidence, or the use of two or more adjacent crystals in the "sum-coincidence" mode. Representative descriptions of sodium iodide spectrometers in which one or both of these methods of continuum suppression have been applied are given in Refs. 7–11.

An explanation of these techniques will be postponed until Chapter 12, where their use with Ge(Li) detectors is detailed. Although significant improvements in peak-to-continuum ratios can be achieved by applying these methods to NaI(Tl) spectrometers, current attention has focused on their application to Ge(Li) systems where continua are much more prominent and greater gains can be achieved through their suppression.

2. THE COMPTON SPECTROMETER

The combination of two separated gamma ray detectors operated in coincidence, as shown in Fig. 10-9, is another configuration that can simplify the response function at the expense of detection efficiency. A collimated beam of gamma rays is allowed to strike the first detector in which the desired mode of interaction is now Compton scattering. Some fraction of the scattered gamma rays will travel to the second detector where they may also interact to give a second pulse. Because the separation distance is normally no greater than a few tens of centimeters, the pulses are essentially in time coincidence. By selectively recording only those pulses from the first crystal that are in coincidence with a pulse from the second crystal, the recorded spectrum largely reflects only single Compton scattering events. Because the angle of scattering is fixed, a constant amount of energy is deposited for each scattering interaction involving monoenergetic incident gamma rays. Photoelectric absorption and all other events which do not lead to coincidence between the two detectors are excluded. The response function is thus reduced to a single peak which appears at a position within the original Compton continuum determined by the scattering angle.

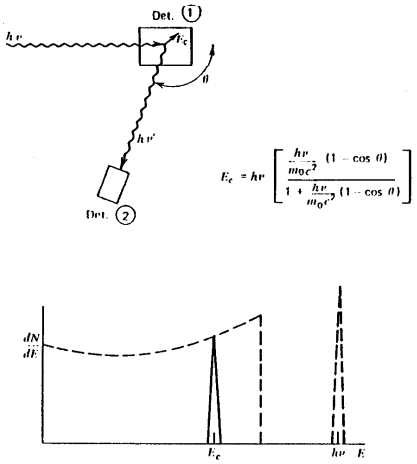

FIGURE 10-9. The geometry of the Compton spectrometer is shown at the top. The spectrum of events from detector ① which are in coincidence with pulses from detector ② is shown as the solid curve at the bottom. The normal spectrum from detector ① is shown as the dashed curve.

IV. PROPERTIES OF NaI(Tl) SCINTILLATION SPECTROMETERS

A. Response Function

The relative importance of each response function feature described in the previous section depends on the gamma ray interaction probabilities in the detector material. NaI is an attractive material choice because the high atomic number ($Z = 53$) of its iodine constituent assures that photoelectric absorption will be a relatively important process. Of all the practical gamma ray spectrometers developed to date, this material shows a comparatively large photofraction and a high intrinsic detection efficiency. The importance of many of the factors that influence the shape of the response function for NaI(Tl) scintillators is detailed by Mueller and Maeder[12].

An extensive catalog of experimentally measured gamma ray spectra for nearly 300 radionuclides as recorded by a 3″×3″ NaI(Tl) spectrometer has been published by Heath[5]. A later compilation by Adams and Dams[6] contains

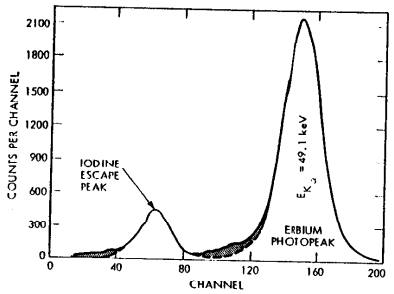

FIGURE 10-10. A low-energy spectrum from a NaI(Tl) scintillator for incident 49.1 keV X-rays from erbium. The iodine characteristic X-ray escape peak lies 25 keV below the photopeak. (From Dell and Ebert[13].)

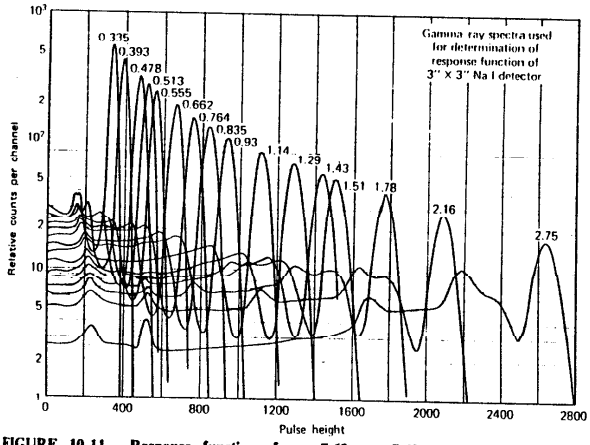

FIGURE 10-11. Response functions for a 7.62 cm×7.62 cm cylindrical NaI(Tl) scintillator for gamma rays from 0.335–2.75 MeV. (From Heath[5].)

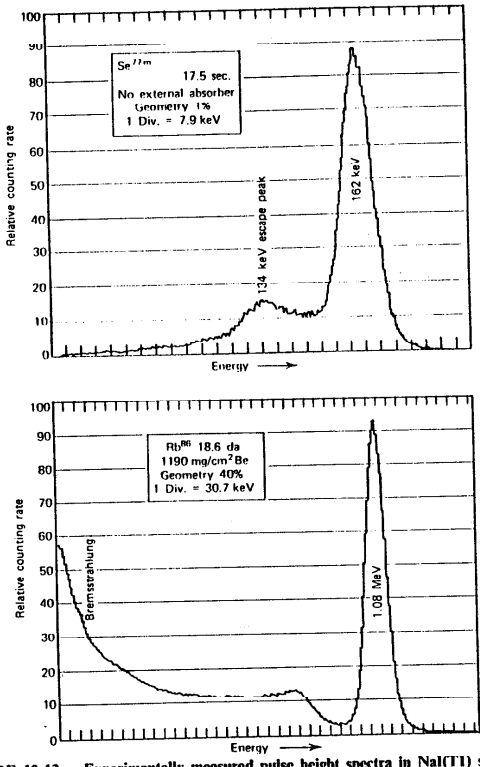

FIGURE 10-12. Experimentally measured pulse height spectra in NaI(Tl) scintillators for two radioisotopes emitting monoenergetic gamma rays. The top spectrum shows the iodine X-ray escape peak which can be evident for gamma rays of relatively low energy. The bottom spectrum, for a higher energy gamma ray, shows the bremsstrahlung generated by stopping the beta particles within the source, in addition to the Compton continuum and photopeak (From F. Adams and R. Adams, *Applied Gamma-Ray Spectrometry*, 2nd ed. Copyright 1970 by Pergamon Press, Ltd. Used with permission.)

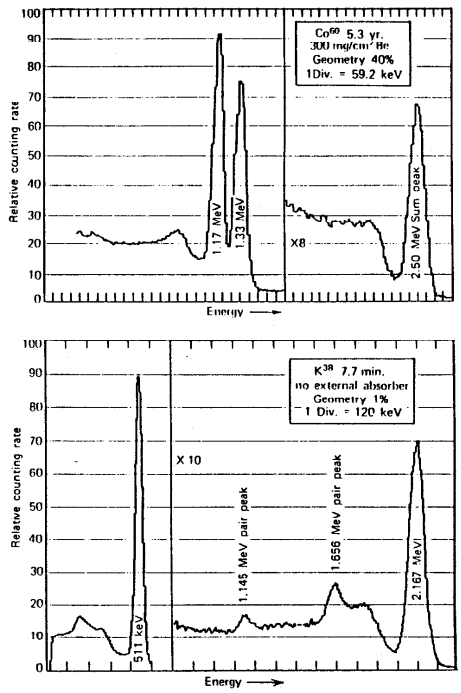

FIGURE 10-13 (a) Experimentally measured pulse height spectrum for ^{60}Co (1.17 and 1.33 MeV gamma rays) from a 10.16 cm × 10.16 cm cylindrical NaI(Tl) scintillator. The large fractional solid angle of 40 percent subtended by the detector enhances the sum peak intensity. (b) Spectrum from ^{38}K (2.167 MeV gamma ray plus positron annihilation photons) from a 7.62 cm × 7.62 cm NaI(Tl) scintillator. The single and double escape peaks for the high-energy gamma ray are evident, as well as a backscatter peak at ~200 keV. (From F. Adams and R. Dams, *Applied Gamma-Ray Spectrometry*, 2nd ed. Copyright 1970 by Pergamon Press, Ltd. Used with permission.)

spectra for both 3″×3″ and 4″×4″ cylindrical sodium iodide crystals. These published data can be of considerable help in predicting the response function to be expected from a scintillation spectrometer when applied to gamma ray emitting isotopes. Examples of gamma ray spectra taken from these compilations are given in Figs. 10-10 through 10-13. Many of the features described in the previous discussion can be observed in these spectra.

Because of the lack of suitable sources, it is often difficult to experimentally measure the response function for all gamma ray energies of potential interest. It is then necessary to resort to calculations to derive the response function. Because of the complexity of the situation in which multiple interactions play an important role, virtually all practical calculations are done using the Monte Carlo method. The work of Berger and Seltzer[14] is a good example of such a calculation for sodium iodide cylindrical detectors. This publication also contains an extensive list of references to prior experimental and calculational efforts. Figure 10-14 shows the good match to experimental data which can be obtained when the computational model contains sufficient detail to adequately represent all important interactions taking place within the detector. Figure 10-15 illustrates a set of calculated response functions for a sodium iodide scintillator extending to relatively high gamma ray energies. The gradual disappearance of the photopeak and the broadening of the escape peaks as the gamma ray energy increases is clearly illustrated by this series of plots. The photopeak disappears because pair production becomes the dominant mode of interaction, and the high-energy pair which is produced is difficult to fully

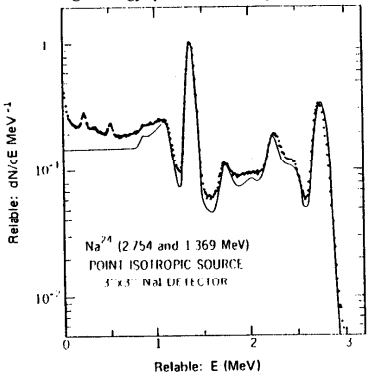

FIGURE 10-14. A comparison of a measured pulse height spectrum (points) with a theoretical spectrum calculated by Monte Carlo methods. (From Berger and Seltzer[14].)

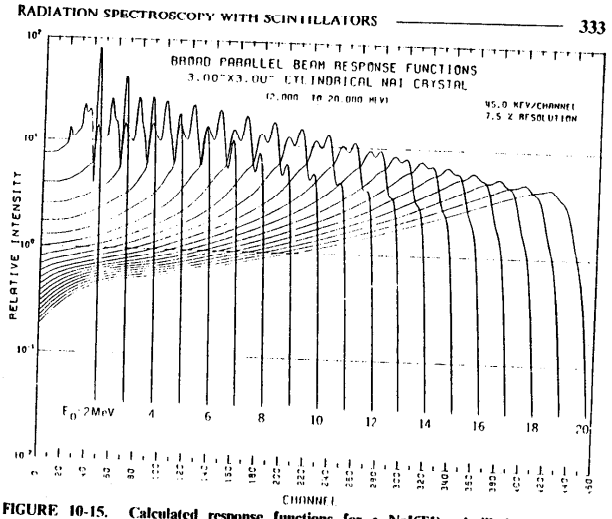

FIGURE 10-15. Calculated response functions for a NaI(Tl) scintillation detector extending to 20 MeV. (From Berger and Seltzer[14].)

absorb due to losses from bremsstrahlung emission and leakage from the surface of the crystal. The broadening of the escape peak is due to the additional statistical fluctuations in the number of photoelectrons produced as their number increases (see Sec. B.2 below.)

B. Energy Resolution

In contrast to the theoretical energy deposition spectra shown in Figs. 10-2 to 10-4, the measured response functions shown above contain the "blurring" effects due to the finite energy resolution of the detector. The most striking difference is the fact that all peaks now have some finite width rather than appearing as narrow, sharp lines.

As introduced in Chapter 3, the *energy resolution* R is defined as

$$R = \frac{FWHM}{H_0} \qquad (10\text{-}14)$$

where

$FWHM$ = full width at half maximum of the full energy peak
H_0 = mean pulse height corresponding to the same peak

The energy resolution of scintillators is the poorest of any commonly used detector, and therefore the spectra have relatively broad peaks.

1. ORIGINS OF RESOLUTION LOSS

From the arguments of Chapter 3, the finite energy resolution of any detector may contain contributions due to the separate effects of charge collection statistics, electronic noise, variations in the detector response over its active volume, and drifts in operating parameters over the course of the measurement. For scintillation detectors, the fluctuations in photomultiplier tube gain from event to event (see Chapter 9, III D) can also add to the measured resolution. For the majority of applications of sodium iodide scintillators to gamma ray spectroscopy, the first of these sources is normally the most significant. Contributions of electronic noise are usually negligible, so that preamplifiers and other electronic components used with scintillators need not include elaborate schemes for noise reduction. Variations in the light collected from scintillation events over the volume of the crystal can be a significant problem, so the techniques discussed in Chapter 8 for promoting uniform light collection are quite important. In commercially prepared crystals of typical sizes, these nonuniformities normally are a small part of the total peak width. Drifts in the operating parameters are usually associated with the photomultiplier tube and can be severe if the detector is subject to large changes in counting rate or temperature. Some methods of spectrum stabilization discussed in Chapter 18 can be applied in these cases, but usually are necessary only under extreme conditions.

2. PHOTOELECTRON STATISTICS

Statistical spreads are therefore left as the single most important cause of peak broadening in sodium iodide scintillators. The statistical fluctuations will be most significant at the point in the signal chain at which the numbers of information carriers are at a minimum. For scintillators, this point is reached after conversion of the scintillation light to electrons by the photocathode of the photomultiplier tube.

A representative numerical example is helpful in illustrating this point. In the signal chain illustrated below, it is assumed that exactly 0.5 MeV of electron energy is deposited by the gamma ray photon in the scintillation crystal. In thallium activated sodium iodide, the scintillation efficiency is about 13 percent. In the example, 65 keV is thus converted by the scintillator into visible light with an average photon energy of about 4 eV. Therefore, about 15 000 scintillation photons are produced per pulse. With allowance for some light loss at the crystal surface and at the crystal-phototube interface, perhaps 10 000 of these light photons ultimately reach the photocathode. If we assume that the average quantum efficiency of the photocathode over the scintillation spectrum is 20 percent, then 2000 photoelectrons are produced. This number is now the minimum in the signal chain because subsequent stages in the photomultiplier tube multiply the number of electrons.

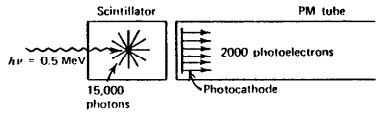

The amplitude of the signal produced by the photomultiplier tube is proportional to this number of photoelectrons. For repeated events in which exactly the same energy is deposited in the crystal, the pulse amplitude will fluctuate due to the inherent statistical variation in the number of photoelectrons collected for each event. If we assume that Poisson statistics hold, then the standard deviation of the number of photoelectrons should be the square root of the mean number produced. Therefore, in our example we would expect a standard deviation of $\sqrt{2000}$, or about 2.2 percent of the mean value. Energy resolution is formally defined in terms of the full width at half maximum of the peak rather than its standard deviation. For an assumed Gaussian shape, the $FWHM$ is 2.35 values of the standard deviation, and therefore the statistical contribution to the energy resolution for the example should be 5.2 percent.

In many practical cases, the statistical broadening of the peak predominates over other potential sources of resolution loss. In that event, the variation of the resolution with gamma ray energy can be predicted simply by noting that the $FWHM$ of the peak is proportional to the square root of the gamma ray photon energy. The average pulse height produced is directly proportional to the gamma ray energy. Therefore, from the definition of energy resolution,

$$R \equiv \frac{FWHM}{H_0} = K\frac{\sqrt{E}}{E} = \frac{K}{\sqrt{E}} \qquad (10\text{-}15)$$

The energy resolution should thus be inversly proportional to the square root of the gamma ray energy. If we take logarithm of both sides of Eq. 10-15, we derive

$$\ln R = \ln K - \frac{1}{2}\ln E \qquad (10\text{-}16)$$

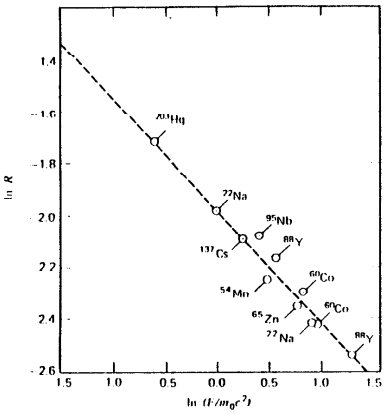

FIGURE 10-16. Experimentally measured resolution R from an NaI(Tl) scintillation detector for various gamma ray energies E. (From Beattie and Byrne[15].)

Therefore, a plot of $\ln R$ versus $\ln E$ should be a straight line with slope of $-1/2$.

Figure 10-16 shows a plot of experimentally determined resolution values for a sodium iodide scintillator as a function of the gamma ray energy at which they were measured. The data adhere fairly closely to a straight line, but the slope is not as steep as predicted, indicating the influence of nonstatistical sources of the peak broadening. A more adequate representation of measured data can take the form

$$R = \frac{(\alpha + \beta E)^{1/2}}{E} \tag{10-16}$$

where α and β are constants particular to any specific scintillator-photomultiplier combination.

3. OTHER FACTORS IN ENERGY RESOLUTION

Other sources of resolution loss in scintillation spectrometers are conveniently categorized into three groups: those that are characteristic of the crystal itself (the "intrinsic crystal resolution"), those effects that are characteristic of the photomultiplier tube, and the variable probability that a visible photon gener-

ated by a scintillation event in the crystal produces a photoelectron which is collected by the first dynode of the PM tube ("the transfer variance").

The intrinsic crystal resolution includes any variation caused by local fluctuations in the scintillation efficiency of the crystal. With modern fabrication techniques, the uniformity of sodium iodide crystals is generally sufficiently good so that the line broadening due to this effect alone would be very small (less than 2 percent). More significant fluctuations arise because of the less-than-perfect reflection conditions that exist at the surface of the crystal. The consequent nonuniform light collection efficiency can introduce significant line broadening, especially in crystals of large size.

The variance introduced by the photomultiplier tube can be a significant contribution. Uniformity of photoelectron collection from the photocathode is an important factor, as is the statistical fluctuation in the electron multiplication. There is considerable variation in the performance of different photomultipliers in this regard, even among different samples of the same design. For example, in a study of several hundred PM tubes sampled from a few standard types, Persyk and Moi[16] observed an average NaI scintillator energy resolution of 10–11 percent for ^{57}Co radiation (122 keV). The best PM tube included in the sample, however, gave a corresponding value of 8.5 percent.

A more subtle component of the intrinsic crystal resolution arises from the slight nonlinearity of sodium iodide scintillation response (see Fig. 8-8). If all incident gamma rays underwent an interaction in which their entire energy were converted to a single electron, this nonlinearity would not be a source of resolution loss. However, the incident gamma ray energy may be subdivided among two or more secondary electrons through single or multiple Compton scattering followed by photoelectric absorption. Furthermore, even if simple photoelectric absorption occurs, the excited atom that remains may convert its excitation energy in a number of ways which lead to varying electron energy spectra, primarily in the form of Auger electrons. Consequently, even a monoenergetic flux of incident gamma rays will lead to a wide distribution of electron energies within the crystal. If the response of the crystal is not linear with electron energy, the total light yield will be different from event to event, depending on details of the energy subdivision between the various electrons that are produced. These effects appear to be significant for gamma ray energies above a few hundred keV for which multiple interactions are predominant, and have been studied in detail by Narayan and Prescott[17].

Because the energy resolution varies with energy, values are usually specified at a fixed gamma ray energy for intercomparison purposes. It is conventional to quote the energy resolution for gamma rays from ^{137}Cs (0.662 MeV) as a standard. The energy resolution for other gamma ray energies can then be estimated through the use of Eqs. 10-15 or 10-16.

Good quality solid sodium iodide scintillators coupled to modern photomultiplier tubes can achieve an energy resolution of about 6–7 percent at 0.662 MeV.

If the shape of the crystal is more complicated than a simple right cylinder, the added difficulty of uniformity in light collection will often make the resolution somewhat worse. For example, the energy resolution for crystals with a center well is generally 1–3 percent larger than the equivalent solid cylinder.

4. PREVENTION OF RESOLUTION LOSS DUE TO LONG-TERM DRIFT

In measurements with scintillators that must extend over many hours or days, some resolution loss can be experienced due to drifts in the gain of the photomultiplier tube and other circuit components. Some electronic methods which can be used to minimize or completely eliminate these effects are outlined in Chapter 18. These techniques work best when there is a single isolated peak in the spectrum from which an error signal can be derived to adjust a variable gain component in the signal chain. If a strong isolated peak does not exist in the measured spectrum, or if the counting rates are low, these methods may be impractical.

For scintillation counters, an alternative method can be used which is based on providing a reference light source within the scintillation package to produce an artificial peak in the spectrum. If the light pulses are of constant intensity, a feedback signal can be generated to adjust the system gain to hold the resulting peak at a constant position on the measured spectrum. Light sources used for this purpose fall into two general categories: those that consist of a combination of a radioactive isotope with a suitable phosphor, and those that are basically electronic in design. A common requirement is that their yield be extremely stable over long periods of time because any change in light output will be interpreted as a drift in the gain of the counting system. Discussions of the design of light sources used for this purpose are given in Refs. 18–21.

C. Linearity

For all scintillators, the "scintillation efficiency" or amount of light generated per unit energy loss (dL/dE) depends both on the particle type and its kinetic energy. For an ideal spectrometer, dL/dE would be a constant independent of particle energy. The total light yield would then be directly proportional to the incident particle energy, and the response of the scintillator would be perfectly linear.

For electrons in NaI(Tl), the scintillation efficiency does vary with electron energy (see Fig. 8-8). The dependence is relatively mild, however, and when coupled with the fact that monoenergetic gamma rays will produce different combinations of electron energies in the crystal, leads to an average pulse height versus gamma ray energy which does not deviate greatly from linearity.

Figure 10-17 shows some experimental results for linearity measurements on NaI(Tl). This nonlinearity must be taken into account when relating the pulse height scale to gamma ray energy. In practice, a calibration is usually carried out in which peak positions are plotted versus known gamma ray energies. Because Fig. 10-17 represents the slope of this calibration line, a small degree of curvature or nonlinearity should be expected. For interpolation between narrowly spaced peaks of known energy, however, assumption of linearity normally leads to a negligible error.

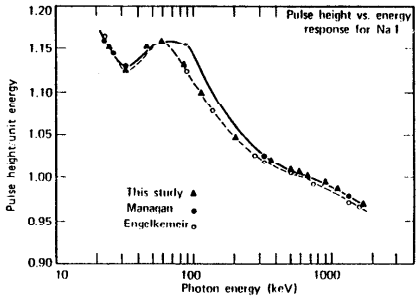

FIGURE 10-17. The differential linearity measured for an NaI(Tl) scintillator. (From Heath[5].)

D. Detection Efficiency

One of the marked advantages in using scintillation crystals for gamma ray measurements is the fact that many standard size detectors can be mass produced with virtually identical properties. Because the physical dimensions of these crystals can be controlled to within very small tolerances, the interaction probability for gamma rays will be identical for all crystals of the same size and shape.

One of the common applications of sodium iodide scintillators is to measure the absolute intensity of a given source of gamma rays. From the discussion in Chapter 3, such a measurement based on simple counting data requires a prior knowledge of the efficiency of the radiation detector. Undoubtedly there are more published data available on the detection efficiency of sodium iodide scintillators for gamma rays than for any other detector type or application. The number of different sizes and shapes of NaI(Tl) crystals in routine use is relatively limited so that reasonably complete data can be compiled on each of the common configurations.

1. CRYSTAL SHAPES

Two general shapes of crystals are in widespread use for applications in gamma ray detection. The solid right circular cylinder is simple to manufacture and encapsulate, and can be mounted directly to the circular face plate of most photomultiplier tubes. If the height-to-diameter ratio of the cylinder does not

greatly exceed unity, the light collection properties are quite favorable in this geometry. If the height-to-diameter ratio is much less than one, the pulse height resolution can often be improved by interposing a light pipe between the crystal and photomultiplier tube to spread the light more uniformly from each scintillation event over the entire photocathode, and thereby average out spatial variations of its quantum efficiency.

A *well crystal* is a right circular cylinder into which a cylindrical well has been machined, usually along the cylindrical axis. A significant advantage of this geometry is the very high counting efficiency that can be achieved by placing the samples to be counted at the bottom of the well. In this position, almost all of the gamma rays that are emitted isotropically from the source are intercepted by at least a portion of the crystal. For low-energy gamma rays, the counting efficiency in this geometry can therefore approach 100 percent. At higher energies, some of the advantage is lost because the average path length through the crystal is somewhat less than if the gamma rays were externally incident on a solid crystal. Because the efficiency for sources near the bottom of the well is not a sensitive function of position, well counters can also simplify the counting of multiple samples with different physical properties while providing nearly identical counting efficiency.

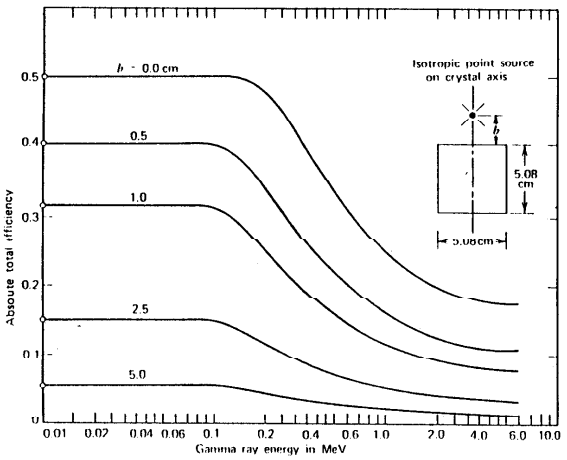

FIGURE 10-18. The absolute total efficiency calculated for a 5.08 cm × 5.08 cm solid cylindrical NaI(Tl) scintillator. Different values of the source location are shown. (From Snyder[22].)

2. EFFICIENCY DATA

Data on detector efficiency are commonly presented in the form of a graph of the efficiency value as a function of gamma ray energy. Some examples are shown in Figs. 10-18 through 10-21. It is important to point out those parameters that must be specified before using this type of data:

1. The specific category of efficiency which is being tabulated must be clearly identified. As defined in Chapter 3, detector efficiencies are classified as either absolute or intrinsic, with the latter being the more common choice. An additional specification must be made that deals with the type of event which is accepted by the counting system. Here the most common choices are either peak or total efficiencies, with the distinction hinging on whether only full-energy events or all events are accepted (see Chapter 3).

2. The size and shape of the scintillation crystal have a strong influence on the counting efficiency. Although the major influence on the intrinsic efficiency is the thickness of the crystal in the direction of the incident gamma radiation, mild variation with other detector dimensions should also be expected.

3. The size and physical nature of the source also influence the counting efficiency. Data are widely available for the relatively simple case of an

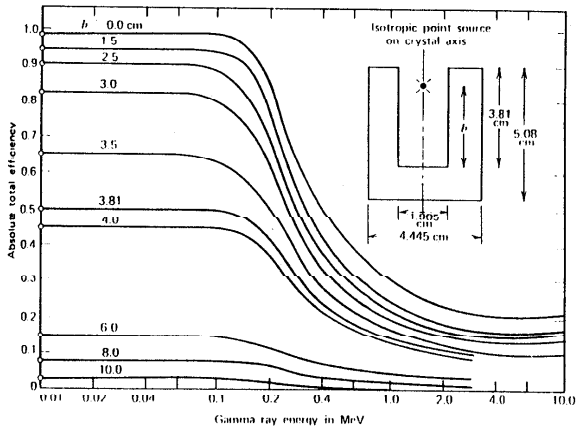

FIGURE 10-19. The absolute total efficiency calculated for point gamma ray source and a NaI(Tl) well-type scintillator with the dimensions shown. The parameter *h* is the source height above the well bottom. (From Snyder[22].)

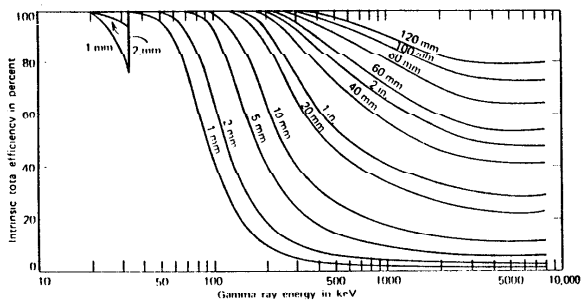

FIGURE 10-20. The intrinsic total efficiency of various thicknesses of NaI(Tl) for gamma rays perpendicular to its surface.

isotropic point gamma ray source located a specified distance from the detector face along its axis. Although absolute efficiencies are quite sensitive to the source-detector spacing, this dependence is much milder for intrinsic efficiencies and vanishes entirely if the source is sufficiently far from the detector. Other common source conditions for which data can be found include the case of a parallel beam of gamma rays uniformly irradiating one surface of the detector (equivalent to a point source at an infinite distance) and a narrowly collimated beam (a "pencil beam") incident at a specified point on the detector surface. Limited data also are available for distributed sources consisting of discs or volumetric sources under specified source-detector geometries.

4. Any absorption taking place between the point of gamma ray emission and the scintillation crystal will also influence the detection efficiency. Published data normally neglect the effects of the crystal housing and other material between the source and detector, but some data can be found which account for self-absorption within large-volume gamma ray sources.

There are two general methods by which efficiency data may be generated. The most straightforward is simply to measure the appropriate counting rate induced by a gamma ray source of known activity. Sets of "standard" gamma ray sources can be purchased whose absolute activity can be quoted to about 1 percent precision. If the experimenter has a set of such sources available covering the energy range of interest, then an efficiency curve can be experimentally determined for the specific detector in use. In many cases, however, a set of

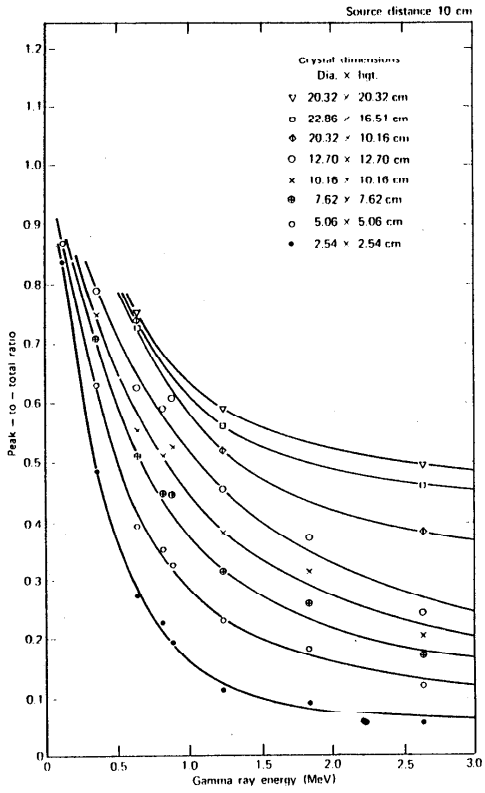

FIGURE 10-21. Peak-to-total ratio (or the "photofraction") for various solid cylinders of NaI(Tl), for a point gamma ray source 10 cm from the scintillator surface. (Courtesy Harshaw Chemical Company.)

absolutely calibrated sources is not available or they do not adequately represent the geometric irradiation conditions of the actual experiment. Then the experimenter must turn to published efficiency data which can include a greater variety of energies and experimental conditions.

A second means of obtaining efficiency data is through calculation based on an assumed knowledge of the various gamma ray interaction probabilities. The simplest case is the total efficiency, which is completely determined by the total linear absorption coefficient μ which characterizes the detector material. The intrinsic total efficiency is just the value of the gamma ray interaction probability ($1-e^{-\mu l}$) integrated over all path lengths l taken by those gamma rays that strike the detector. For simple geometries, this integration can be carried out analytically. In most cases, however, the peak efficiency is of greater interest. Because more complex processes involving multiple interactions contribute to full-energy events, the peak efficiency, in general, no longer can be calculated analytically. Instead, recourse must be made to Monte Carlo calculations which attempt to simulate the behavior of gamma ray photons based on knowledge of the individual probabilities for photoelectric absorption, Compton scattering, and pair production. Because each Monte Carlo calculation is, in effect, a computer experiment, the results obtained are subject to statistical uncertainties determined by the number of histories that have been calculated. Furthermore, the results are specific to the detector geometry and gamma ray energy assumed, and cannot be further generalized.

Extensive tables and graphs of sodium iodide detector efficiencies can be found in Refs. 5, 6, and 23. A good review of both experimentally determined and calculated efficiencies for solid cylindrical sodium iodide crystals has recently been published by Grosswendt and Waibel[24]. Extensive references are also tabulated in Refs. 25 and 26 for calculations and measurements of efficiencies for well-type crystals, and in Ref. 27 for other crystal shapes.

When the gamma ray emitting sample is not negligibly small, self-absorption effects can substantially reduce the efficiency that would be obtained for point sources. The usual procedure is to apply a multiplicative corrrection factor to standard efficiencies to account for absorption within the sample itself. This approach has been shown to adequately represent a wide range of physical situations[28]. Reviews of scintillator efficiencies for absorbing disc sources are given in Refs. 29 and 30.

Most of the available efficiency data concerns sources that are located along the axis of symmetry of the detector, and only limited data are available regarding the directional response of scintillation crystals to off-axis sources. One such analysis for cylindrical scintillators is given in Ref. 31, which also contains references to other previously published data on directional characteristics.

Efficiency data on scintillation materials other than sodium iodide are also relatively scarce. Cesium iodide is probably the next most common choice for gamma ray spectroscopy, and Figs. 10-22 and 10-23 present some data for its

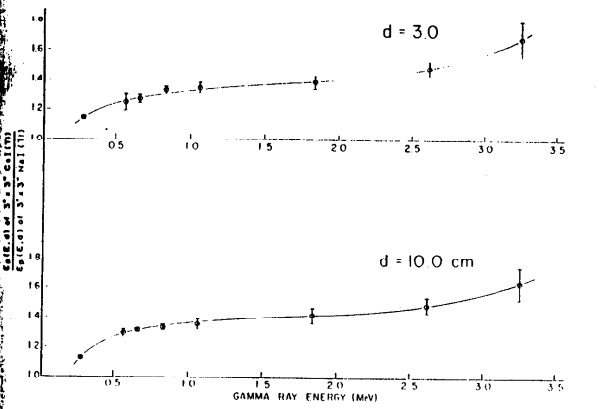

FIGURE 10-22. Relative intrinsic peak efficiencies of 7.62 cm×7.62 cm cylindrical crystals of CsI(Tl) and NaI(Tl); d is the crystal-to-source distance. (From Irfan and Prasad[32].)

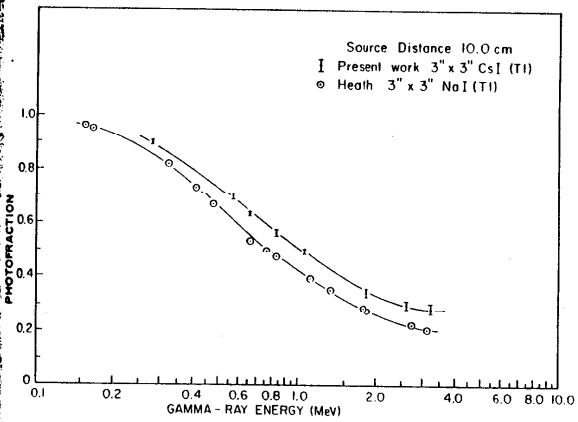

FIGURE 10-23. Experimental photofractions of 7.62 cm×7.62 cm cylindrical crystals of CsI(Tl) and NaI(Tl). (From Irfan and Prasad[32].)

intrinsic efficiency and photofraction relative to a sodium iodide crystal of the same size. Cesium iodide exhibits both a higher efficiency and a greater photofraction, but its somewhat lower light output (see Chapter 8) leads to a poorer energy resolution. Gamma ray detection efficiency for NE-213 organic liquid scintillators are given in Refs. 33 and 34, and for lead-doped plastic scintillators in Ref. 35.

3. PEAK AREA DETERMINATION

In order to apply the peak efficiency data for any detector, the area under the full-energy peaks that appear in its spectrum must be determined. Even after subtraction of the normal background, nearly all such peaks will be superimposed on a continuum caused by many of the complicating effects described earlier in this chapter. It is therefore not always a simple task to determine the number of events that contribute to a given full-energy peak.

If the peak were a simple isolated one without any superimposed continuum, as shown in Fig. 10-24a, its area could be determined by simple integration between the limits shown. When the spectrum is recorded in a multichannel analyzer, the equivalent process is a simple addition of the content of each channel between the indicated limits. If a continuum is also present, as in Fig. 10-24b, some additional unwanted counts are included in this process, and must be subtracted. Some shape must therefore be assumed for the continuum within the region under the peak, and a number of fitting procedures of varying degrees of complexity can be applied. A linear interpolation between the continuum values on either side of the peak is the easiest approach and will give sufficient accuracy for many purposes.

At times, closely spaced or overlapping peaks do not allow the straightforward summation method to be applied. More complex methods must then be used to separate the individual contributions of each of the closely lying peaks. These methods normally involve fitting an analytic shape to that portion of the peak which can be clearly resolved, and assuming that the remainder of the peak is described by the fitted function. It has been demonstrated[36] that a Gaussian curve fitted to the points that lie within one standard deviation on either side of the peak value adequately represents the shape of the measured photopeak from a NaI(Tl) scintillator over an assortment of source geometry and counting conditions. More complex shapes are sometimes necessary for spectra recorded at high rates or under nonideal circumstances. Because a good deal of complexity is involved in such fitting routines, nearly all are carried out by computer programs which are described in further detail in Chapter 18.

V. ELECTRON SPECTROSCOPY WITH SCINTILLATORS

Scintillators can also be applied to the measurement of fast electrons (such as beta particles) which are incident on one surface of the crystal. Although it has become more common to use lithium-drifted silicon detectors for this purpose

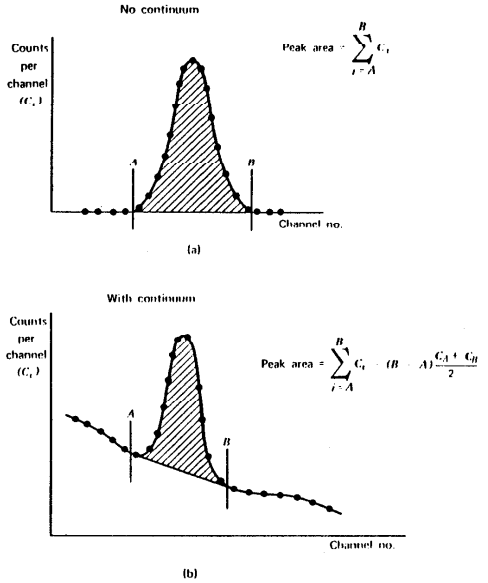

FIGURE 10-24. Methods of obtaining peak areas from multichannel spectra.

(see Chapter 13), applications sometimes arise in which the size limitation of silicon detectors or other considerations dictate the use of scintillators.

The nature of the electron response function depends on the scintillation material, its physical thickness, and the angle of incidence of the electrons. Electrons from an external source normally must pass through some protective covering and/or light reflector before reaching the surface of the scintillator itself. In the discussion that follows, the energy loss that may occur in these intervening materials is not explicitly considered, but may be important if the electron energy is small. We will also assume that the scintillators under consideration are thicker than the maximum range of the incident electrons. Even so, the detector may not be totally opaque to the secondary bremsstrahlung photons which will be generated along the path of the electron.

In general, the response functions show a pronounced full-energy peak corresponding to the total absorption of the incident electron energy, together with a tail extending to lower energies. The major cause of such partial energy absorption is "backscattering," in which the electron re-emerges from the surface through which it entered after having undergone only partial energy loss. Other events that contribute to the tail are those electrons which are fully stopped within the scintillator, but which generate bremsstrahlung photons that escape from the front or back surface of the detector.

Both the probability of backscattering and the fraction of the electron energy loss to bremsstrahlung increase markedly with the atomic number of the scintillator. Because both of these processes detract from the full-energy peak and add the unwanted tail to the response function, scintillators with low atomic number are generally preferred for electron spectroscopy (just the opposite criterion than that desired for gamma ray spectroscopy). Therefore, organic

TABLE 10-1. Fraction of Normally Incident Electrons which Are Backscattered from Various Detector Surfaces

	Electron energy (MeV)				
Scintillator	0.25	0.50	0.75	1.0	1.25
Plastic	0.08 ± 0.02	0.053 ± 0.010	0.040 ± 0.007	0.032 ± 0.003	0.030 ± 0.005
Anthracene	0.09 ± 0.02	0.051 ± 0.010	0.038 ± 0.004	0.029 ± 0.003	0.026 ± 0.004
NaI(Tl)	0.450 ± 0.045	0.410 ± 0.010	0.391 ± 0.014	0.375 ± 0.008	0.364 ± 0.007
CsI(Tl)	0.49 ± 0.06	0.455 ± 0.023	0.430 ± 0.013	0.419 ± 0.018	0.404 ± 0.016

From Titus[37].

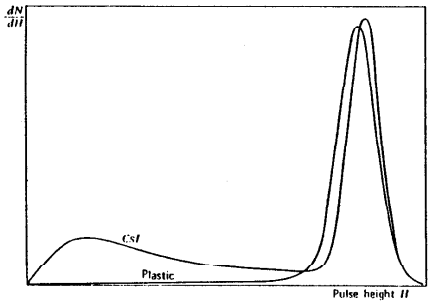

FIGURE 10-25. Experimental pulse height spectra from CsI(Tl) and plastic scintillators for 1.0 MeV electrons at normal incidence. The spectra are normalized to the same maximum pulse height. (From Titus[37].)

scintillators such as anthracene or plastics are most commonly applied in electron measurements. Table 10-1 lists the probability for backscattering of normally incident electrons from some common scintillator materials. The much lower backscattering probabilities for the low-Z materials are evident.

Figure 10-25 shows measured pulse height spectra in both cesium iodide and a plastic scintillator for normally incident 1 MeV electrons. The low energy tail is more pronounced for cesium iodide because of its higher atomic number. Additional data for other scintillation materials, electron energies, and varying angles of incidence are given in Ref. 37.

VI. SPECIALIZED DETECTOR CONFIGURATIONS BASED ON SCINTILLATION

A. The Phoswich Detector

The combination of two dissimilar scintillators optically coupled to a single photomultiplier tube is often called a "phoswich" (or phosphor sandwich) detector. The scintillators are chosen to have different decay times so that the shape of the output pulse from the photomultiplier tube is dependent on the relative contribution of scintillation light from the two scintillators. Most applications involve the use of this pulse shape difference to distinguish events that have occurred in only one scintillator from those that occur in both. For example, lightly penetrating radiations can be made to stop fully in the first scintillator, but more penetrating particles may generate light in both. Sodium iodide and cesium iodide are often chosen as the two materials because their decay times are quite different (0.25 and 1.1 μs), and pulses arising from only one decay are easily distinguished from those with both components, using the pulse shape discrimination methods of Chapter 17. Phoswich detectors have proved to be useful in the low-background counting of X-rays and beta particles[38].

B. The Moxon-Rae Detector

Another type of gamma ray detector can be built based on the detection of secondary electrons produced by gamma ray interactions in a converter which is external to the detector. Although the resulting detection efficiency is typically quite low, the efficiency versus energy dependence can be tailored in certain ways to suit the need of specialized applications. For example, Moxon and Rae[39] first described the properties of a thick low-Z converter used to produce secondary electrons which were then detected by a thin plastic scintillator. By choosing a converter which consisted of graphite with a small component of bismuth, they found that the detection efficiency could be made nearly proportional to the incident gamma ray energy. This proportionality allows a simplified analysis to be carried out for a class of experiments involving neutron capture because the detection probability of any given radiative capture event becomes independent of the specific de-excitation cascade mechanisms following the

capture[39]. The proportionality of efficiency with gamma ray energy results from the combined probabilities of electron production within the converter and of their escape from the surface facing the electron detector. Detailed analyses of the theory and performance of Moxon-Rae detectors can be found in Refs. 39–41.

C. Liquid Scintillation Counters

The liquid scintillation media discussed in Chapter 8 can be applied to avoid some of the difficulties that arise when measuring low-energy beta particles or alphas using conventional methods. The approach, sometimes called *internal source liquid scintillation counting*, involves dissolving the sample to be counted directly in the liquid scintillator. Under these conditions, problems relating to sample self-absorption, attenuation of particles by detector windows, and beta backscattering from the detector are completely avoided. These advantages are particularly important for low-energy radiations such as the beta particles emitted by tritium and ^{14}C. The endpoint energies for these beta spectra are 18 keV and 160 keV, respectively, and average beta energies are about half these values. Because these isotopes are particularly important in chemical and biomedical applications, much of the development of the liquid scintillation technique has taken place in connection with these sciences. Several texts have been published[42–44] which thoroughly review the fundamental principles of liquid scintillation counting. Proceedings of conferences dedicated to various applications in this field can be found in Refs. 45–47.

The first step in the technique involves incorporation of the sample within a suitable liquid scintillation solution. Problems can often arise in this step because most liquid scintillation solutions are based on toluene or other organic solvent, whereas many samples are often more conveniently prepared in an aqueous solution. Detailed discussions of various methods for obtaining stable solutions through the use of solublizing or complexing agents are given in Refs. 48 and 49. A common problem is that the introduction of the sample tends to reduce the scintillation light output compared with the pure scintillator. This phenomena, commonly called *quenching*, often limits the amount of sample material that can be effectively incorporated within the scintillator solution. The quenching can be due either to alteration of the optical properties of the solution by the sample ("color quenching") or through interference with the energy transfer process within the scintillator itself. Insoluble materials can sometimes be introduced as a suspension of fine particles. In those cases where rapid settling of the suspension is a problem, some methods have been developed which involve converting the solution to a gel immediately after preparation of these suspensions.

After the sample has been prepared, the solution is normally loaded into a glass vial and placed in a light-tight enclosure viewed by one or more photomultiplier tubes. Because of the effects of quenching and the fact that typical

applications involve radiations of low energy, pulses produced in the photomultiplier tube often correspond to no more than a few photoelectrons. Under these circumstances, the measurements are potentially very sensitive to sources of noise that may interfere with accurate and reproducible counting of the sample. Significant sources of noise are thermally generated photoelectrons from the photocathode of the PM tube, long-lived phosphorence in the scintillator, and "chemiluminescence" (light generated by chemical reactions within the sample-scintillator solution). Virtually all these noise sources correspond to the generation of only a single photoelectron per pulse, so they can normally be rejected by placing a discrimination level in the signal chain to eliminate those pulses whose amplitude correspond to a single photoelectron. However, because the signal also consists of only a few photoelectrons, there is a risk that this discrimination process will also eliminate some of the signal.

Because all beta particles emitted by the sample pass through some portion of the scintillator, and the great majority are fully stopped within the solution, the counting efficiency can potentially be close to 100 percent. The degree to which the few-photoelectron signal can be distinguished from single-electron noise determines the practical counting efficiency. As a gauge of the development of the technique, it is interesting to note the improvement in the counting efficiency for tritium as improvements in photomultiplier tube design and other techniques have been implemented. A counting efficiency of about 20 percent in 1960 was improved to about 60 percent in 1970 through the use of low-noise bialkali photomultiplier tubes, and to about 90 percent at the time of this writing through the application of PM tubes with gallium phosphide high-gain dynodes[50].

One method of eliminating the photomultiplier tube noise is to use two PM tubes to view the scintillator from opposite sides. Only those pulses that are observed in coincidence between the two tubes are counted. Because the noise generated in each tube will be uncorrelated, a true coincidence will not be observed for these events, and the recorded counts will correspond only to events generated within the liquid scintillator. The summed output from both photomultiplier tubes can then be used to record the pulse height spectrum from the sample.

Although most commonly applied to samples emitting beta particles or conversion electrons, liquid scintillation counting has also been used to count samples that are alpha active[51–53]. Although the best reported energy resolution of 5–8 percent[52] is much inferior to that attainable with semiconductor diode detectors, the advantages of high counting efficiency and uniform counting geometry offer some attraction for applications such as counting low-level environmental samples[53]. Because typical alpha energies are several MeV, the light output is much greater than for low-energy beta particle counting, and therefore a counting efficiency that approaches 100 percent is relatively easy to achieve. Pulse shape discrimination can be applied to eliminate backgrounds due to beta particles or gamma ray induced events[54]. Using these techniques, an

exceptionally low background level of 0.01 counts/min has been reported[52] while maintaining essentially 100 percent counting efficiency for alpha particles within the sample.

PROBLEMS

10-1. A gamma ray photon after Compton scattering through an angle of 90° has an energy of 0.5 MeV. Find its energy before the scattering.

10-2. A 2 MeV gamma ray photon is incident on a detector, undergoes two sequential Compton scatterings, and then escapes. If the angles of scattering are 30° and 60°, respectively, how much total recoil electron energy is deposited in the detector?

Does the answer change if the sequence of the scattering angles is reversed?

10-3. The cross sections for photoelectric, Compton, and pair production interactions in sodium iodide at 2 MeV are in the ratio 1:20:2, respectively. Will the pulse height spectrum from 2 MeV gammas incident on a sodium iodide scintillator give a peak-to-total ratio of less than, more than, or about equal to 1/23?

10-4. If the energy resolution of a particular NaI(Tl) scintillation detector is 7 percent for ^{137}Cs gamma rays (0.662 MeV), estimate its energy resolution for the 1.28 MeV gamma rays from ^{22}Na.

10-5. The mass attenuation coefficient of NaI at 0.5 MeV is 0.955 cm^2/g. Find the intrinsic total efficiency of a slab detector 2.54 cm thick at this energy. If the photofraction is 40 percent at the same energy, what is the intrinsic peak efficiency?

10-6. (a) Find the energy of the Compton edge for the 1.17 MeV gamma rays from ^{60}Co.

(b) Calculate the backscatter peak energies corresponding to incident gamma rays of 1 MeV, 2 MeV, and 3 MeV.

10-7. Listed below are a number of parameters of interest in gamma ray spectroscopy using scintillation detectors:

(a) Density of the detector medium
(b) Kinetic energy required to create a scintillation photon in the crystal
(c) Average atomic number (Z-value) of the detector medium
(d) Geometry of the source detector system
(e) Gain of the photomultiplier tube
(f) Quantum efficiency of the photocathode in the photomultiplier
(g) Gain of the amplifier used between the detector and pulse analysis system
(h) Fraction of light generated in the crystal that reaches the photocathode of the PM tube (light collection efficiency)

Identify those parameters from this list that have a major influence on the detector *intrinsic peak efficiency*. Repeat, but now identify those that have a major influence on *energy resolution*.

10-8. Calculate the pulse amplitude from the anode of a photomultiplier tube used with a NaI(Tl) scintillator under the following conditions:

A 1 MeV electron loses all its energy in the scintillator, the light collection efficiency to the photocathode is 50 percent, the average quantum efficiency of the photocathode is 20 percent, and 80 percent of the photoelectrons are collected at the first dynode. Assume that the PM tube has 10 stages with a multiplication factor $\delta = 2.5$ per stage. The anode load resistance is 100 kΩ, and the anode capacitance is 100 pF.

10-9. A particular radioisotope emits two coincident gamma rays, each with 100 percent yield per decay, with no angular correlation between the photon directions. A sample is placed 10 cm from the surface of a 5 cm-radius cylindrical detector along its axis. The intrinsic peak efficiency of the detector for γ_1 is 50 percent, and for γ_2 it is 30 percent.

(a) If the sample activity is low enough so that chance coincidences are negligible, calculate the ratio of the counts under the sum peak in the recorded pulse height spectrum to the counts under the γ_1 full-energy peak.

(b) Calculate the rate at which events are recorded in the sum peak if the source activity is 100 kBq. For a detector resolving time of 3 μs, what additional rate should be expected from chance coincidences between γ_1 and γ_2?

REFERENCES

1. J. B. Birks, *The Theory and Practice of Scintillation Counting*, Pergamon Press, Oxford (1964).
2. S. M. Shafroth, Ed., *Scintillation Spectroscopy of Gamma Radiation*, Gordon & Breach, London (1967).
3. K. Siegbahn, Ed., *Alpha-, Beta-, and Gamma-Ray Spectroscopy*, North Holland Pub. Co., Amsterdam, 1968.
4. C. D. Broyles, D. A Thomas, and S. K Haynes, *Phys. Rev. 89*, 715 (1953).
5. R. L. Heath, *Scintillation Spectrometry Gamma-Ray Spectrum Catalogue*, IDO-16880, Volumes 1 and 2 (1964).
6. F. Adams and R. Dams, *Applied Gamma-Ray Spectrometry*, 2nd Edition and revision of original publication by C. E. Crouthamel, Pergamon Press, Oxford (1970).
7. N. A. Wogman, D. E. Robertson, and R. W. Perkins, *Nucl. Instr. and Meth., 50*, 1 (1967).
8. N. A. Wogman, R. W. Perkins, and J. H. Kaye, *Nucl. Instr. and Meth. 74*, 197 (1969).

9. B. A. Euler, D. F. Covell, and S. Yamamoto, *Nucl. Instr. and Meth., 72*, 143 (1969).
10. B. Bengtson and M. Moszynski, *Nucl. Instr. and Meth., 85*, 133 (1970).
11. M. D. Hasinoff, S. T. Lim, D. F. Measday, and T. J. Mulligan, *Nucl. Instr. and Meth., 117*, 375 (1974).
12. R. Mueller and D. Maeder, "Single Crystal Spectroscopy," Ch. VII in *Scintillation Spectroscopy of Gamma Radiation*, S. M. Shafroth, Ed., Gordon and Breach, New York, 1967.
13. J. R. Dell and P. J. Ebert, *Nucl. Instr. and Meth., 68*, 335 (1969).
14. M. J. Berger and S. M. Seltzer, *Nucl. Instr. and Meth., 104*, 317 (1972).
15. R. J. D. Beattie and J. Byrne, *Nucl. Instr. and Meth., 104*, 163 (1972).
16. D. E. Persyk and T. E. Moi, *IEEE Trans. Nucl. Sci.*, NS 25, No. 1, 615 (1978).
17. G. H. Narayan and J. R. Prescott, *IEEE Trans. Nucl. Sci.*, NS 15, No. 3, 162 (1968).
18. H. J. Fraser, *Nucl. Instr. and Meth., 136*, 513 (1976).
19. J. Uyttenhove, et al., *Nucl. Instr. and Meth., 141*, 549 (1977).
20. P. N. Johnson and D. W. L. Tolfree, *Nucl. Instr. and Meth., 134*, 29 (1976).
21. C. L. Morris, W. J. Braithwaite, and C. F. Moore, *Nucl. Instr. and Meth., 136*, 197 (1976).
22. B. J. Snyder, "Calculation of Gamma Ray Scintillation Detector Efficiencies and Photofraction by Monte Carlo Methods," Ph.D. Dissertation, The University of Michigan, 1965.
23. C. C. Grosjean and W. Bossaert, *Table of Absolute Detection Efficiencies of Cylindrical Scintillation Gamma-Ray Detectors*, Computing Lab., Univ. of Ghent (1965).
24. B. Grosswendt and E. Waibel, *Nucl. Instr. and Meth., 133*, 25 (1976).
25. P. Holmberg and R. Rieppo, *Int. Jour. Appl. Rad. and Iso. 24*, 99 (1973).
26. R. Rieppo, *Int. Jour. Appl. Rad. and Iso., 27*, 453 (1976).
27. R. Rieppo, *Nucl. Instr. and Meth., 115*, 541 (1974).
28. Y. S. Horowitz, S. Mordechai, and A. Dubi, *Nucl. Instr. and Meth., 122*, 399 (1974).
29. T. Nakamura, *Nucl. Instr. and Meth., 105*, 77 (1972).
30. M. Belluscio, R. De Leo, A. Pantaleo, and A. Vox, *Nucl. Instr. and Meth., 118*, 553 (1974).
31. I. Petr, A. Adams, and J. B. Birks, *Nucl. Instr. and Meth., 95*, 253 (1971).
32. M. Ilan and R. D. G. Prasad, *Nucl. Instr. and Meth., 107*, 583 (1973).
33. N. A. Lurie, L. Harris, Jr., and J. P. Wondra, *Nucl. Instr. and Meth., 129*, 619 (1975).
34. R. De Leo, G. D'Erasmo, and A. Pantaleo, *Nucl. Instr. and Meth., 129*, 501 (1975).
35. A. Schaarschmidt and H. Durner, *Nucl. Instr. and Meth., 105*, 504 (1972).
36. T. S. Mudhole and N. Umakantha, *Nucl. Instr. and Meth., 116*, 401 (1974).
37. F. Titus, *Nucl. Instr. and Meth., 80*, 93 (1970).
38. M. R. Mayhugh, A. C. Lucas, and B. K. Utts, *IEEE Trans. Nucl. Sci.*, NS-25, No. 1, 569 (1978).

39. M. C. Moxon and E. R. Rae, *Nucl. Instr. and Meth., 24*, 445 (1963).
40. S. S. Malik, *Nucl. Instr. and Meth., 125*, 45 (1975).
41. S. S. Malik and C. E. Majkrzak, *Nucl. Instr. and Meth., 130*, 443 (1975).
42. Y. Kobayashi and D. V. Maudsley, *Biological Applications of Liquid Scintillation Counting*, Academic Press, New York (1974).
43. D. L. Horrocks, *Applications of Liquid Scintillation Counting*, Academic Press, New York (1974).
44. M. Crook and P. Johnson, Eds., *Liquid Scintillation Counting*, Vol. 4, Heyden and Son, London (1977).
45. P. E. Stanley and B. A. Scoggins, *Liquid Scintillation Counting: Recent Developments*, Academic Press, New York (1974).
46. A. A. Noujaim, C. Ediss, and L. I. Wiebe, *Liquid Scintillation Science and Technology*, Academic Press, New York (1976).
47. D. L. Horrocks and C. T. Peng, Eds., *Organic Scintillators and Liquid Scintillation Counting*, Academic Press, New York (1971).
48. J. H. Parmentier and F. E. L. Ten Haaf, *Int. Jour. Appl. Rad. and Iso. 20*, 305 (1969).
49. B. W. Fox, *Techniques of Sample Preparation for Liquid Scintillation Counting*, North-Holland Pub. Co., Amsterdam (1976).
50. R. Vaninbroukx and I. Stanef, *Nucl. Instr. and Meth., 112*, 111 (1973).
51. J. W. McKlveen, H. W. Berk, and W. R. Johnson, *Int. Jour. Appl. Rad. and Iso. 23*, 337 (1972).
52. J. W. McKlveen and W. J. McDowell, *Trans. Am. Nuc. Soc. 22*, 149 (1975).
53. W. J. McDowell, *IEEE Trans. Nucl. Sci.*, NS 22, No. 1, 649 (1975).
54. P. Cross and G. W. McBeth, *Health Physics 30*, 303 (1976).

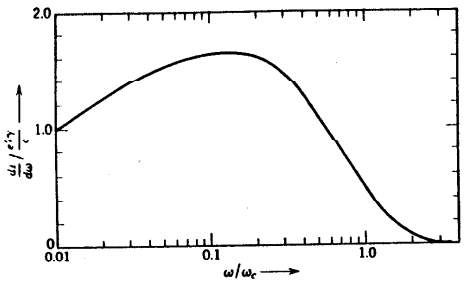

Fig. 14.11 Synchrotron radiation spectrum (energy radiated per unit frequency interval) as a function of frequency. The intensity is measured in units of $\gamma e^2/c$, while the frequency is expressed in units of ω_c (14.85).

the fundamental frequency $\omega_0 = c/\rho$. Since the charged particle repeats its motion at a rate of $c/2\pi\rho$ revolutions per second, it is convenient to talk about the angular distribution of power radiated into the nth multiple of ω_0 instead of the energy radiated per unit frequency interval per passage of the particle. To obtain the harmonic power expressions we merely multiply $dI/d\omega$ (14.95) or $d^2I/d\omega\, d\Omega$ (14.83) by the repetition rate $c/2\pi\rho$ to convert energy to power, and by $\omega_0 = c/\rho$ to convert per unit frequency interval to per harmonic. Thus

$$\left.\begin{aligned} \frac{dP_n}{d\Omega} &= \frac{1}{2\pi}\left(\frac{c}{\rho}\right)^2 \frac{d^2I}{d\omega\, d\Omega}\bigg|_{\omega=n\omega_0} \\ P_n &= \frac{1}{2\pi}\left(\frac{c}{\rho}\right)^2 \frac{dI}{d\omega}\bigg|_{\omega=n\omega_0} \end{aligned}\right\} \tag{14.96}$$

These results have been compared with experiment at various energy synchrotrons.* The angular, polarization, and frequency distributions are all in good agreement with theory. Because of the broad frequency distribution shown in Fig. 14.11, covering the visible, ultraviolet, and X-ray regions, synchrotron radiation is a useful tool for the study of the optical properties of solids. Several synchrotron light facilities exist as parasitic installations attached to high-energy synchrotrons or storage rings whose main purpose is the study of fundamental particles. The article by Godwin† details synchrotron radiation from this point of view.

* F. R. Elder, R. V. Langmuir, and H. C. Pollock, *Phys. Rev.*, **74**, 52 (1948); D. H. Tomboulain and P. L. Hartman, *Phys. Rev.*, **102**, 1423 (1956); G. Bathow, E. Freytag, and R. Haensel, *J. Appl. Phys.*, **37**, 3449 (1966).

† R. P. Godwin, in *Springer Tracts in Modern Physics*, Vol. 51, ed. G. Höhler, Springer-Verlag, Berlin (1969), pp. 1–73.

Synchrotron radiation has been observed in the astronomical realm associated with sunspots, the Crab nebula, and from the particle radiation belts of Jupiter. For the Crab nebula the radiation spectrum extends over a frequency range from radiofrequencies into the extreme ultraviolet, and shows very strong polarization. From detailed observations it can be concluded that electrons with energies ranging up to 10^{12} eV are emitting synchrotron radiation while moving in circular or helical orbits in a magnetic induction of the order of 10^{-3} gauss (see Problem 14.15). The radio emission at $\sim 10^3$ MHz from Jupiter comes from energetic electrons trapped in Van Allen belts at distances from a few to 30–100 radii (R_J) from Jupiter's surface. Data from a space vehicle (Pioneer 10, December 4, 1973 encounter with Jupiter) passing within $2.8R_J$ showed a roughly dipole magnetic field with a dipole moment of $4R_J^3$ gauss. Appreciable fluxes of trapped electrons with energies greater than 3 MeV and a few percent with energies greater than 50 MeV were observed. Taking 1 gauss as a typical field and 5 MeV as a typical energy, Eqs. (12.42) and (14.85) show that the spiraling radius is of the order of 100–200 meters, $\omega_0 \sim 2\times 10^6\ \text{sec}^{-1}$, and that about 10^3 significant harmonics are radiated.

14.7 Thomson Scattering of Radiation

If a plane wave of monochromatic electromagnetic radiation is incident on a free particle of charge e and mass m, the particle will be accelerated and so emit radiation. This radiation will be emitted in directions other than that of the incident plane wave, but for nonrelativistic motion of the particle it will have the same frequency as the incident radiation. The whole process may be described as scattering of the incident radiation.

According to (14.20) the instantaneous power radiated into polarization state $\boldsymbol{\epsilon}$ by a particle of charge e in nonrelativistic motion is

$$\frac{dP}{d\Omega} = \frac{e^2}{4\pi c^3}|\boldsymbol{\epsilon}^* \cdot \dot{\mathbf{v}}|^2 \tag{14.97}$$

The acceleration is provided by the incident plane wave. If its propagation vector is $\mathbf{k}_0$, and its polarization vector $\boldsymbol{\epsilon}_0$, the electric field can be written

$$\mathbf{E}(\mathbf{x}, t) = \boldsymbol{\epsilon}_0 E_0 e^{i(\mathbf{k}_0 \cdot \mathbf{x} - \omega t)} \tag{14.98}$$

Then, from the force equation for nonrelativistic motion, we have the acceleration,

$$\dot{\mathbf{v}}(t) = \boldsymbol{\epsilon}_0 \frac{e}{m} E_0 e^{i(\mathbf{k}_0 \cdot \mathbf{x} - \omega t)} \tag{14.99}$$

If we assume that the charge moves a negligible part of a wavelength during one cycle of oscillation, the time average of $|\dot{\mathbf{v}}|^2$ is $\frac{1}{2}\text{Re}\,(\dot{\mathbf{v}} \cdot \dot{\mathbf{v}}^*)$. Then the average

power per unit solid angle can be expressed as

$$\left\langle \frac{dP}{d\Omega} \right\rangle = \frac{c}{8\pi} |E_0|^2 \left(\frac{e^2}{mc^2}\right)^2 |\epsilon^* \cdot \epsilon_0|^2 \tag{14.100}$$

Since the process is most simply viewed as a scattering, it is convenient to introduce a scattering cross section, as in Chapter 9 defined by

$$\frac{d\sigma}{d\Omega} \simeq \frac{\text{Energy radiated/unit time/unit solid angle}}{\text{Incident energy flux in energy/unit area/unit time}} \tag{14.101}$$

The incident energy flux is just the time-averaged Poynting vector for the plane wave, namely, $c\,|E_0|^2/8\pi$. Thus from (14.100) we obtain the differential scattering cross section,

$$\frac{d\sigma}{d\Omega} = \left(\frac{e^2}{mc^2}\right)^2 |\epsilon^* \cdot \epsilon_0|^2 \tag{14.102}$$

The scattering geometry with a choice of polarization vectors for the outgoing wave is shown in Fig. 14.12. The polarization vector ϵ_1 is in the plane containing $\mathbf{n}$ and $\mathbf{k}_0$; ϵ_2 is perpendicular to it. In terms of unit vectors parallel to the coordinate axes, ϵ_1 and ϵ_2 are

$$\epsilon_1 = \cos\theta(\mathbf{e}_x \cos\phi + \mathbf{e}_y \sin\phi) - \mathbf{e}_z \sin\theta$$

$$\epsilon_2 = -\mathbf{e}_x \sin\phi + \mathbf{e}_y \cos\phi$$

For an incident linearly polarized wave with polarization parallel to the x axis, the angular distribution summed over final polarizations is $(\cos^2\theta\cos^2\phi + \sin^2\phi)$, while for polarization parallel to the y axis it is $(\cos^2\theta\sin^2\phi + \cos^2\phi)$. For unpolarized incident radiation the scattering cross section is therefore

$$\frac{d\sigma}{d\Omega} = \left(\frac{e^2}{mc^2}\right)^2 \cdot \tfrac{1}{2}(1+\cos^2\theta) \tag{14.103}$$

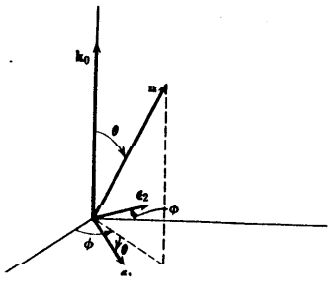

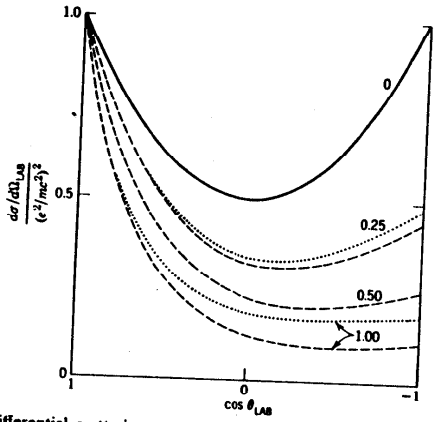

Fig. 14.13 Differential scattering cross section of unpolarized radiation by a point charged particle initially at rest in the laboratory. The solid curve is the classical Thomson result. The dashed curves are the quantum-mechanical results for a spinless particle, with the numbers giving the values of $\hbar\omega/mc^2$. For $\hbar\omega/mc^2 = 0.25$, 1.0 the dotted curves show the results for spin $\frac{1}{2}$ point particles (electrons).

This is called the *Thomson formula* for scattering of radiation by a free charge, and is appropriate for the scattering of X-rays by electrons or gamma rays by protons. The angular distribution is as shown in Fig. 14.13 by the solid curve. The total scattering cross section, called the *Thomson cross section*, is

$$\sigma_T = \frac{8\pi}{3}\left(\frac{e^2}{mc^2}\right)^2 \tag{14.104}$$

The Thomson cross section is equal to 0.665×10^{-24} cm^2 for electrons. The unit of length, $e^2/mc^2 = 2.82\times10^{-13}$ cm, is called the *classical electron radius*, since a classical distribution of charge totaling the electronic charge must have a radius of this order if its electrostatic self-energy is to equal the electron mass.

The classical Thomson formula is valid only at low frequencies where the momentum of the incident photon can be ignored. When the photon's momentum $\hbar\omega/c$ becomes comparable to or larger than mc, modifications occur. These can be called quantum-mechanical effects since the concept of photons as massless particles with momentum and energy is certainly quantum mechanical (*pace*, Newton!), but granting that, most of the modifications are purely

incident energy because the charged particle recoils during the collision. Applying two-body relativistic kinematics to the process, we find that the ratio of the outgoing to the incident wave number is given by the Compton formula,

$$\frac{k'}{k}=\frac{1}{1+\frac{\hbar\omega}{mc^2}(1-\cos\theta)}$$

where θ is the scattering angle in the laboratory (the rest frame of the target). A quantum-mechanical calculation of the scattering of photons by *spinless* point particles of charge e and mass m yields the cross section,

$$\frac{d\sigma}{d\Omega}=\left(\frac{e^2}{mc^2}\right)^2\left(\frac{k'}{k}\right)^2|\boldsymbol{\epsilon}^*\cdot\boldsymbol{\epsilon}_0|^2 \tag{14.105}$$

to be compared with the classical expression (14.102). In the radiation gauge the quantum-mechanical matrix element is the same as the classical amplitude. The factor $(k'/k)^2$ comes entirely from the phase space. Its presence causes the differential cross section to decrease relative to the Thomson result at large angles, as shown by the dashed curves in Fig. 14.13. Also shown in the figure by the dotted curves are the quantum-mechanical results for photon-electron scattering, that is, the scattering by a point spin $\frac{1}{2}$ particle described by the Dirac equation. The curves are generally similar to those for spinless particles, but are somewhat larger at large angles because of scattering by the electron's magnetic moment.* The integral over angles of (14.105) is elementary but slightly involved. We quote only the limiting forms for $\hbar\omega\ll mc^2$ and $\hbar\omega\gg mc^2$:

$$\frac{\sigma}{\sigma_T}=\begin{cases}1-2\dfrac{\hbar\omega}{mc^2}+\cdots, & \hbar\omega\ll mc^2\\[2ex] \dfrac{3}{4}\dfrac{mc^2}{\hbar\omega}, & \hbar\omega\gg mc^2\end{cases} \tag{14.106}$$

For scattering by electrons the low frequency limit is the same, but at high frequencies there is an additional multiplicative factor, $[\frac{1}{2}+\frac{1}{2}\ln(2\hbar\omega/mc^2)]$.

For protons the departures from the Thomson formula occur at photon energies above about 100 MeV. This is far below the critical energy $\hbar\omega\sim Mc^2\sim$ 1 GeV which would be expected in analogy with the electron Compton effect. The reason is that a proton is not a point particle like the electron with nothing but electromagnetic interactions, but is a complex entity having a spread-out charge distribution with a radius of the order of 0.8×10^{-13} cm caused by strong interactions with pi mesons. The departure (a rapid increase in cross section) from Thomson scattering occurs at photon energies of the order of the rest energy of the pi meson (140 MeV).

* For electrons the cross-section equivalent to (14.105) has $|\boldsymbol{\epsilon}^*\cdot\boldsymbol{\epsilon}_0|^2$ replaced by

$$|\boldsymbol{\epsilon}^*\cdot\boldsymbol{\epsilon}_0|^2+\frac{(k-k')^2}{4kk'}\left[1+(\boldsymbol{\epsilon}^*\times\boldsymbol{\epsilon})\cdot(\boldsymbol{\epsilon}_0\times\boldsymbol{\epsilon}_0^*)\right]$$

It is known as the *Klein-Nishina formula* for Compton scattering.

14.8 Scattering of Radiation by Quasi-Free Charges, Coherent and Incoherent Scattering

In the scattering of X-rays by atoms the angular distribution (14.103) is observed at wide angles, at least in light elements. But in the forward direction the scattering per electron increases rapidly to quite large values compared to the Thomson cross section. The reason is a coherent addition of the amplitudes from all electrons. From (14.18) it can be seen that the radiation field from a number of free nonrelativistic charged particles will be

$$\mathbf{E}_a=\frac{1}{c}\sum_j e_j\left[\frac{\mathbf{n}\times(\mathbf{n}\times\dot{\boldsymbol{\beta}}_j)}{R_j}\right]_{\text{ret}} \tag{14.107}$$

With (14.99) for the acceleration of the typical particle, we find

$$\mathbf{E}_a=\frac{E_0}{c^2}\mathbf{n}\times(\mathbf{n}\times\boldsymbol{\epsilon}_0)\sum_j\frac{e_j^2}{m_j}\frac{\exp\left[i\mathbf{k}_0\cdot\mathbf{x}_j-i\omega\left(t-\frac{R_j}{c}\right)\right]}{R_j} \tag{14.108}$$

In calculating the radiation it is sufficient to approximate R_j in the exponent by the form (14.63). Then, in complete analogy with the steps from (14.97) to (14.102), we find the scattering cross section,

$$\frac{d\sigma}{d\Omega}=\left|\sum_j\frac{e_j^2}{m_jc^2}e^{i\mathbf{q}\cdot\mathbf{x}_j}\right|^2\cdot|\boldsymbol{\epsilon}^*\cdot\boldsymbol{\epsilon}_0|^2 \tag{14.109}$$

where

$$\mathbf{q}=\frac{\omega}{c}\mathbf{n}-\mathbf{k}_0 \tag{14.110}$$

is the vectorial change in wave number in the scattering.

Equation (14.109) applies to free charged particles instantaneously at positions $\mathbf{x}_j$. Electrons in atoms, for example, are not free. But if the frequency of the incident radiation is large compared to the characteristic frequencies of binding, the particles can be treated as free while being accelerated by a pulse of finite duration. Thus (14.109) can be applied to the scattering of high-frequency (compared to binding frequencies) radiation by bound charged particles. The only thing that remains before comparison with experiment is to average (14.109) over the positions of all the particles in the bound system. Thus the observable cross section for scattering is

$$\frac{d\sigma}{d\Omega}=\left\langle\left|\sum_j\frac{e_j^2}{m_jc^2}e^{i\mathbf{q}\cdot\mathbf{x}_j}\right|^2\right\rangle|\boldsymbol{\epsilon}^*\cdot\boldsymbol{\epsilon}_0|^2 \tag{14.111}$$

where the symbol $\langle\ \rangle$ means average over all possible values of $\mathbf{x}_j$.